CHALMERS
UNIVERSITY OF TECHNOLOGY

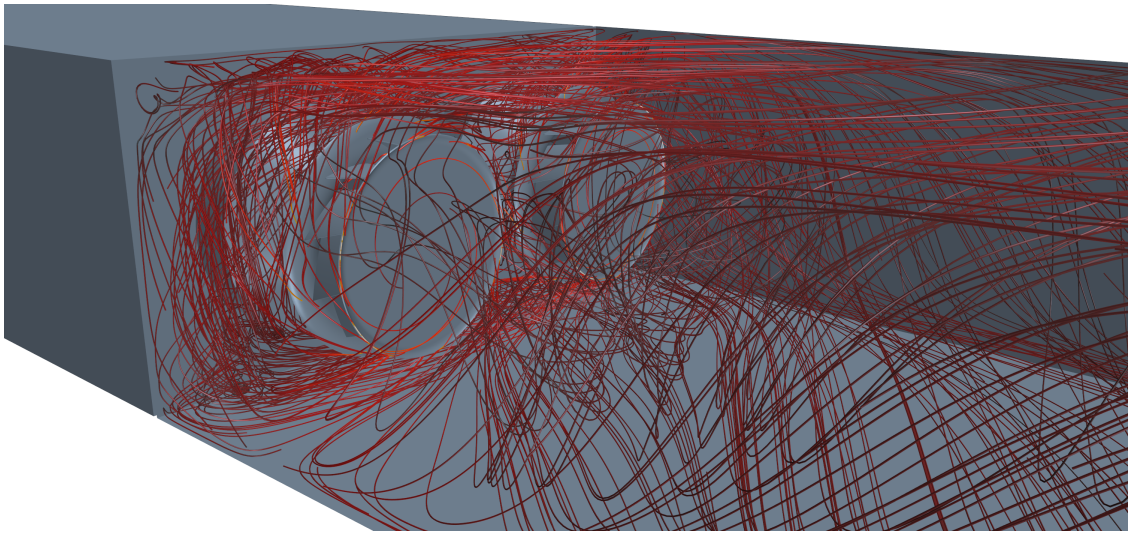

Simulation on centrifugal fans operating at close distance

An investigation of different air handling unit constructions to improve fan efficiency

Master's thesis in Applied Mechanics

FILIP MILIKIC

Department of Mechanics and Maritime Sciences
CHALMERS UNIVERSITY OF TECHNOLOGY
Gothenburg, Sweden 2021

Master's thesis 2021:03

Simulation on centrifugal fans operating at close distance

An investigation of different air handling unit constructions to improve fan efficiency

FILIP MILIKIC

CHALMERS
UNIVERSITY OF TECHNOLOGY

Department of Mechanics and Maritime Sciences
Division of Fluid Mechanics
Chalmers University of Technology
Gothenburg, Sweden 2021

Simulation on centrifugal fans operating at close distance
An investigation of different air handling unit constructions to improve fan efficiency
FILIP MILIKIC

Supervisor: Martin Ottersten, Swegon
Examiner: Lars Davidson, Department of Mechanics and Maritime Sciences

Master's Thesis 2021:03
Department of Mechanics and Maritime Sciences
Division of Fluid Mechanics
Chalmers University of Technology
SE-412 96 Gothenburg
Telephone +46 31 772 1000

Cover: Streamlines of the airflow with a flow rate of 1,0729 m^3/s in the outlet region of the reference case of the AHU.

Department of Mechanics and Maritime Sciences
Gothenburg, Sweden 2021

Simulation on centrifugal fans operating at close distance
An investigation of different air handling unit constructions to improve fan efficiency
FILIP MILIKIC
Department of Mechanics and Maritime Sciences
Chalmers University of Technology

Abstract

To ensure a proper indoor climate, ventilation is of great importance, especially for health reasons. Finding an high energy efficient ventilation unit solution is of big interest for Swegon, the company which initiated this thesis, as it copes with current EU regulations and directives for environmental issues, and at the same time lowers the operating costs. The goal with this study is to run CFD simulations on the current air handling unit, compare the results to three different modifications of the design and determine the potential improvement of the unit in terms of fan efficiency.

The CFD simulations are performed with STAR-CCM+ and experimental tests are performed by Swegon, which are compared to the numerical results. A verification and validation study is performed to ensure mesh independence and realistic results. The results are compared for three different operating points for both methods, with flow rates ranging between 0.90 and 1.26 m^3/s.

Simulation results show that by adding a vertical wall in between the fans, which separates the flows of the fans, the potential increase of the fan efficiency for lower flow rates is up to around 2 %. For larger flow rates the increase is slightly less at around 1.5 %, however still a significant improvement from the current design. In comparison, the experiment results show efficiencies lower for the wall at around 0.5 %.

The main conclusion draw from this study, which is based on both methods, is that the curved wall design shows best potential for energy efficiency, followed by the straight wall and tilted wall, and lastly by the current design.

Keywords: fan efficiency, CFD, air handling unit, centrifugal fan, ventilation, parallel operation.

Acknowledgements

First of all, I would like to thank Swegon AB for making this thesis possible and providing the necessary aid to complete this project. I would like to thank my supervisor Martin Ottersten for providing guidance and support throughout the entire thesis. With his availability, knowledge in the topic and STAR-CCM+, Martin has been a valueable and appreciated resource. Additionally I would like to thank professor Lars Davidson for taking the role as examiner and the study administration at the department of Mechanics and Maritime Sciences for help with regards to administration. Lastly, I would also like to thank family and friends for providing moral support during the entire project.

Filip Milikic, Gothenburg, February 2021

Nomenclature

Abbreviations

AHU	Air Handling Unit
BHP	Brake horsepower
CFD	Computational Fluid Dynamics
CFM	Cubic feet per minute
$HVAC$	Heating, ventilation, and air conditioning
$RANS$	Reynolds-Averaged Navier-Stokes
$V\&V$	Verification and validation

Greek symbols

ϵ	Turbulent dissipation	m^2/s^3
η_{AHU}	AHU efficiency	$-$
κ	Von Kármán constant	$-$
μ	Dynamic viscosity	$kg/(m\,s)$
ω	Rotational speed of fan	rpm
Φ	Viscous-dissipation function	$kg/(m\,s^3)$
ρ	Density	kg/m^3
τ_w	Wall shear stress	Pa

Other symbols

∇	Nabla operator

Roman symbols

Δp_s	Difference in static pressure between inlet and outlet of AHU	Pa
Δs	Near-wall prism layer thickness	m
$\hat{u}$	Internal energy	J
$\mathbf{g}$	Gravity vector	m/s^2
$\mathbf{V}$	Velocity vector	m/s
d_1	Diameter of fan inlet	m
d_2	Diameter of fan outlet	m
E	Error level of pressure between two mesh refinements	$-$

H	Height of AHU casing	m
h_i	Relative step size based on the coarsest mesh	$-$
k	Turbulent kinetic energy	m^2/s^2
L_1	Length of outlet region	m
L_2	Length of inlet region	m
M_{total}	Total moment from both fans	$N\,m$
n	Number of cells for mesh under consideration	$-$
n_0	Number of cells for the coarsest mesh	$-$
P	Power	W
p	Pressure	Pa
p_1	Pressure of coarser mesh under consideration	Pa
p_2	Pressure of finer mesh under consideration	Pa
p_s	Static pressure	Pa
Q	Volume flow	m^3/s
Q_{AHU}	Volume flow in AHU	m^3/s
T	Temperature	K
t	Time	s
u	Velocity in x-direction	m/s
u^+	Dimensionless velocity	$-$
u_t	Friction velocity	m/s
W	Width of AHU casing	m
y	Distance to nearest wall	m
y^+	Dimensionless wall distance	$-$
Z	Number of fan blades	$-$

Contents

List of Figures

List of Tables

1
Introduction

1.1 Background

In indoor environments, it is of great importance for human health to ensure and maintain a good ventilation of the air. A good ventilation system makes sure to get rid of unwanted smells, moisture and dust, but also hazardous gases such as radon, which may cause severe damage to human lungs. [1][2]

Swegon AB is an indoor climate company which is designing and manufacturing ventilation systems. One of their important device is the Air Handling Unit, also known as AHU, which has the purpose to regulate and circulate air in a room or building. The AHU is a large metal box containing a number of different components such as filters, dampers, cooling/heating coils and fans. The main focus of this study will be on the fans. In some of the AHU:s, there are two or more fans operating parallel next to each other. Due to the close distance between the fans, the flow from each fan will interact and cause turbulent losses in the flow, which will cause the static pressure downstream to decrease. The fan efficiency is directly correlated with the static pressure in the AHU, meaning a drop of the fan efficiency is a consequence of this.

In order to lower the energy consumption and reduce cost without compromising with a decrease in existing performance, Swegon is searching for solutions which can improve the fan efficiency. Increasing the efficiency of the fans is of great importance especially out of environmental reasons. In the European Union, there are regulations and directives in use which acts as requirements for the ventilation units and fans. Regulation No. 327/2011 [3] states ecodesign requirements for electric motors used to drive fans and Regulation No. 1253/2014 [4] states ecodesign requirements for ventilation units. These are both based on Directive 2009/125/EC [5], which is an important part of Directive 2018/2002 [6], an updated version of the 20-20-20 goal by EU from 2012, stating that the goal for energy efficiency is set to reach an improvement of 32.5 % by 2030 [7].

This study is a continuation on a previous thesis by Stankic and Ploesteanu [8], who conducted a study in cooperation with Swegon with the goal to improve fan efficiency in an AHU with two fans. The study included an comparison between the initial design and modifications in form of walls, guiding vanes and fan offset. The results showed that the half distance straight wall gave the overall best efficiency improvement.

1.2 Problem statement

The purpose of this study is to identify issues with the current AHU design with two fans and to find out what can be done in order to improve fan efficiency in the design. The main objective is to investigate different concepts and compare them to the current design. The main tasks and goals of the project are to:

- Identify the main sources of pressure loss in the reference case, which in turn is causing the efficiency decrease.
- Design modifications to the existing AHU which might improve the efficiency.
- Determine if the modifications show improvement in terms of efficiency, and in that case by how much, based on CFD-simulations.
- Determine how well the numerical results match the experimental test results.

1.3 Limitations

Due to time and resource limits, the project will be under the following constraints:

- Only the AHU with **two** operating fans will be investigated.
- The shape and geometry of the fans and the AHU are fixed and cannot be altered. This means for instance that changing fan pitch angle or AHU width/height is not allowed.
- The study will mainly focus on the physical results and will only briefly consider other aspects of the results.

2
Theory

In this chapter, the necessary theory behind relevant terms in this study is presented. This involves both theory of fluid mechanics and the application of it in CFD, as well as fan theory, which explains the underlying behavior of the physics of the centrifugal fan.

2.1 Fluid Mechanics

2.1.1 Governing equations

The governing equations used to describe fluid motion consist of the conservation equations for mass (2.1), momentum (2.2) and energy (2.3). The mass conservation law, also known as the continuity equation, ensures that the mass inserted into a control volume is equal to the amount that exits. The momentum conservation law, also known as the Navier-Stokes equations, is derived by Newton's second law of motion and ensures equilibrium between the fluid motion and forces. The energy conservation law is derived from the first law of thermodynamics and ensures equilibrium between the internal energy and fluid forces. [9]

$$\frac{\partial \rho}{\partial t} + \nabla \cdot (\rho \mathbf{V}) = 0 \tag{2.1}$$

$$\rho \frac{D\mathbf{V}}{Dt} = -\nabla p + \rho \mathbf{g} + \mu \nabla^2 \mathbf{V} \tag{2.2}$$

$$\rho \frac{D\hat{u}}{Dt} = -p(\nabla \cdot \mathbf{V}) + \nabla \cdot (k \nabla T) + \Phi \tag{2.3}$$

2.1.2 Turbulent boundary layer

In flows with high Reynolds number where the flow is turbulent, it is of great importance to accurately predict the flow in the turbulent boundary layer. The boundary layer is defined as the layer between the wall up until the flow reaches 99 % of the free stream velocity. Above the limit, in the free stream, the viscous stresses may be neglected. The boundary layer can be split up into two layers: the inner and outer layer. The inner layer can in turn be split up into three sublayers: the viscous layer, the buffer layer and the logarithmic layer. The velocity profile for a turbulent flow near a wall can be seen in Figure 2.1. [10]

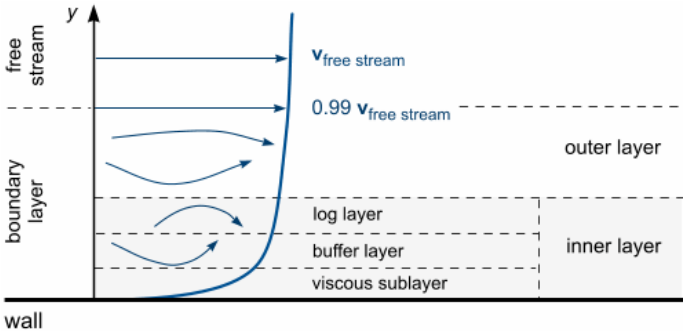

Figure 2.1: Turbulent velocity profile with its different layers and sublayers [10]

In the viscous layer, for $y^+ < 5$, u^+ and y^+ are approximately equal to each other.

$$u^+ = y^+ \tag{2.4}$$

In the logarithmic layer, for $y^+ > 30$, the log-law

$$u^+ = \frac{1}{\kappa} \ln y^+ + B \tag{2.5}$$

is valid to approximate the dimensionless velocity, where the dimensionless values are defined as

$$y^+ = \frac{y u_t}{\nu} \qquad u_t = \sqrt{\frac{\tau_w}{\rho}} \qquad u^+ = \frac{u}{u_t} \tag{2.6}$$

The constants are obtained from experiments for a smooth wall and set as $\kappa = 0.41$ and $B = 5.0$. [9]

In the buffer layer however, for $5 < y^+ < 30$, neither of the two equations give accurate results.

$$u^+ \neq y^+ \qquad u^+ \neq \frac{1}{\kappa} \ln y^+ + B \tag{2.7}$$

The different sublayers for the inner layer and their limits are shown in Figure 2.2.

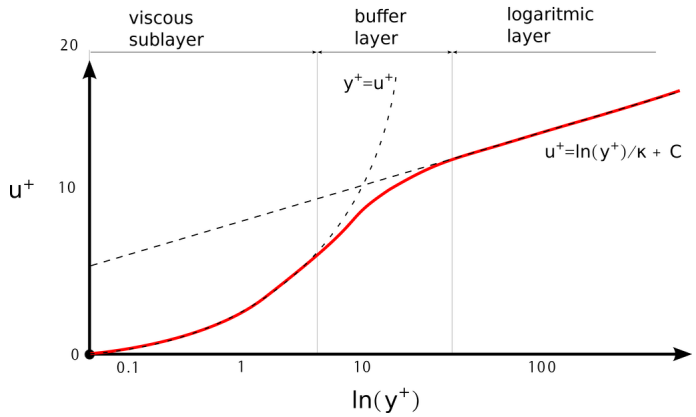

Figure 2.2: Correlation between dimensionless velocity and wall distance for the different sublayers in the inner layer [11]

2.2 Computational Fluid Dynamics

2.2.1 Turbulence modeling

Since the flow in this study has high Reynolds number, it is considered to be turbulent flow and therefore an appropriate turbulence model is needed. The chosen model in this study is the realizable two-layer k-ϵ with all y^+ treatment. The model calculates the turbulent eddy viscosity by solving the transport equations for the turbulent kinetic energy k and turbulent dissipation ϵ. [12]

The two-layer approach is a form which allows the k-ϵ to be used in the viscous layer. As the name suggests, the computation is divided into two layers: one close to the wall and one far from the wall. In the near-wall layer, ϵ and μ_t are functions of the wall distance, and the values are smoothly blended together with the values obtained from the layer far from the wall. [13] This form allows for accurate results for meshes with near-wall cell at either $y^+ \approx 1$ or $y^+ > 30$. In addition to this, the model is combined with the realizable k-ϵ model. The difference from the standard k-ϵ model is a new transport equation for the turbulent dissipation rate, as well as the introduction of a variable damping function which is used to constraint the normal stresses in order to avoid non-physical phenomena. [14][15]

2.2.2 Moving reference frame

This study involves rotating fans, which means the motion has to be modelled. This is modelled by defining a local frame of reference that is moving in a different way compared to the stationary reference frame. This method does not move the mesh vertices, meaning it may only be applied to a steady state simulation, which will provide a solution that is time-averaged.

2.3 Centrifugal fan theory

The purpose with this section is to provide a basic background of the centrifugal fan and its common characteristics. Some of the decisions and arguments made in the study are based on this theory and is therefore important to have in mind.

2.3.1 Construction

The main components of the fan are the shroud, backplate and blades, as shown in Figure 2.3. The blades are located between the shroud and backplate and are spread out in a circular pattern. An inlet duct is connected with the shroud in the upstream region and its purpose is to lead the airflow into the fan.

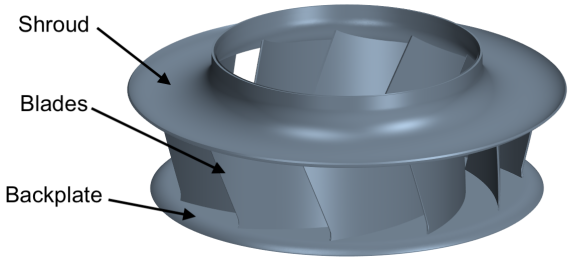

Figure 2.3: Fan geometry and its different components

2.3.2 Operation

The purpose of a centrifugal fan is to increase the static pressure of the air flow. This is obtained by rotating the fan with a constant angular velocity, driven by an electrical motor. When the air moves to the tip of the blade from the hub, the kinetic energy is increased, which is transformed into static pressure in the downstream region, causing a pressure increase compared to the upstream region. [16]

The operation principle of the centrifugal fan is shown in Figure 2.4. In the left figure, the inlet airflow is represented by the red arrows, the outlet airflow by the blue arrows and the rotation of the fan by the yellow arrows. The inlet airflow is directed into the inlet hole by the inlet duct and it has relatively straight flow normal to the inlet when entering the fan. The airflow exiting the fan from the blades in the outlet region however, obtains a rotational behavior due to the rotation of the fan. The increased velocity of the flow and static pressure as explained above, is visualized in the right figure. Each green arrow represents a velocity vector for an individual particle of air. As the blade move for a certain time step, the air particle at the tip of the blade will have moved longer than a particle at the hub, meaning it will have obtained a larger velocity, and in turn larger kinetic energy.

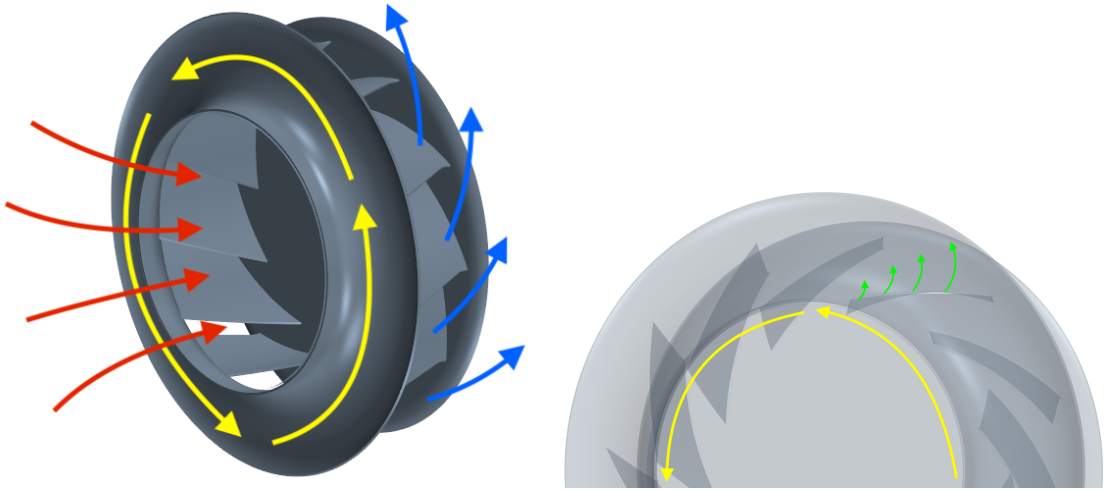

Figure 2.4: Visualization of the operating principles of the centrifugal fan

2.3.3 Affinity laws

The relationship between volume flow, static pressure, power and rotational speed for fans in HVAC applications can be expressed using the affinity laws. These are used in order to estimate characteristics of a fan with different operating conditions than a previously tested fan with known variables. Assuming incompressible flow and no change in fan diameter, the equations are expressed as (subscript 1 stands for tested fan and subscript 2 stands for untested fan):

$$\frac{Q_1}{Q_2} = \frac{\omega_1}{\omega_2} \qquad \frac{p_{s,1}}{p_{s,2}} = \left(\frac{\omega_1}{\omega_2}\right)^2 \qquad \frac{P_1}{P_2} = \left(\frac{\omega_1}{\omega_2}\right)^3 \tag{2.8}$$

In other words, for a given fan diameter, the volume flow is directly proportional to the rotational speed, the static pressure is directly proportional to the square of the rotational speed and the power is directly proportional to the cube of the rotational speed. [17] By keeping the rotational speed constant for both cases, the equations can be rewritten as:

$$\frac{p_{s,1}}{p_{s,2}} = \left(\frac{Q_1}{Q_2}\right)^2 \qquad \frac{P_1}{P_2} = \left(\frac{Q_1}{Q_2}\right)^3 \tag{2.9}$$

2.3.4 Fan efficiency

The equation to determine the fan efficiency is shown in Equation 2.10. It is defined as the ratio between the power transferred to the airflow to the power used by the motor to rotate the fan, also known as brake horsepower (BHP). The power transferred to the airflow is the product of the difference in static pressure between inlet and outlet of AHU, and the volume flow rate at the inlet. The brake horsepower is defined as the product of the total moment of both fans, and the rotational speed of each individual fan. [18]

$$\eta_{AHU} = \frac{\Delta p_s \cdot Q_{AHU}}{BHP} = \frac{\Delta p_s \cdot Q_{AHU}}{M_{total} \cdot \omega} \tag{2.10}$$

2.3.5 Fan performance curves

This section is based on information by US Department of Energy and Air Movement and Control Association [16], and Twin City Fan Companies [19].

The most common and relevant characteristic in fan theory is the relationship between the static pressure and volume flow rate (denoted as CFM in the figures). This relationship can be shown in a fan curve, which is obtained by experimental testing of the fan. Data is collected by setting a range of different volume flows from no flow until the point where the pressure increase is zero, while keeping the rotational speed of the fan constant.

As seen in Figure 2.5, region of low flow rates are producing the largest static pressure. This region is called *Stall region* since it is considered to be unstable. This is a result of cyclic behavior of the fan trying to increase the flow rate, which causes the pressure to increase. This will in turn reduce the generated flow rate, causing the pressure to decrease, leading the fan trying to generate a higher flow. This instability leads to noise, low fan efficiency and fatigue on the fan blades and motor bearing, and should therefore be avoided. The selected flow rate should instead be located somewhere in the right side of the graph, in between the maximum and minimum pressure.

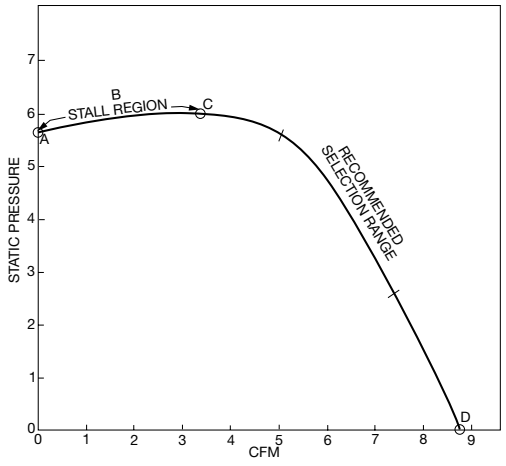

Figure 2.5: Fan curve for a backward inclined centrifugal fan [19]

The fan performance curve, shown in Figure 2.6, is completed by including the system and power curves. The system curve describes the relationship between static pressure and volume flow rate within a given system. It is represented by a parabolic curve as defined in the first expression in Equation 2.9, where the static pressure is equal to the square of the volume flow rate. The point of intersection between the fan and system curves is called *operating point* and is the point of stable equilibrium between fan and system. The power curve (denoted as BHP in the figures) is given as power needed to drive the fan at any given flow rate. The power for any point is found by starting at the operating point and moving vertically up or down (depending on location) until the power curve is reached.

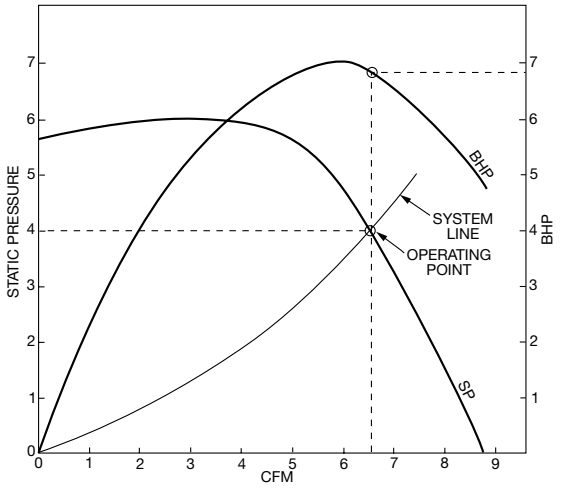

Figure 2.6: Fan, system and power curves for a backward inclined centrifugal fan [19]

However, it is not always the case that the fan operates in the operating point due to higher or lower flow rate obtained than desired. This can be adjusted by increasing or decreasing the rotational speed of the fan according to the affinity laws defined in Equation 2.8. By varying the rotational speed, *operating lines* are obtained which indicate the range of operation along the system curve, as shown in Figure 2.7 (a). The same applies for the power curve, as the operating point will change position in flow rate axis direction. Operating lines can also be obtained by varying system characteristics. This can for instance be made by adding a damper, and will instead cause a range of operating lines along the fan curve, as shown in Figure 2.7 (b).

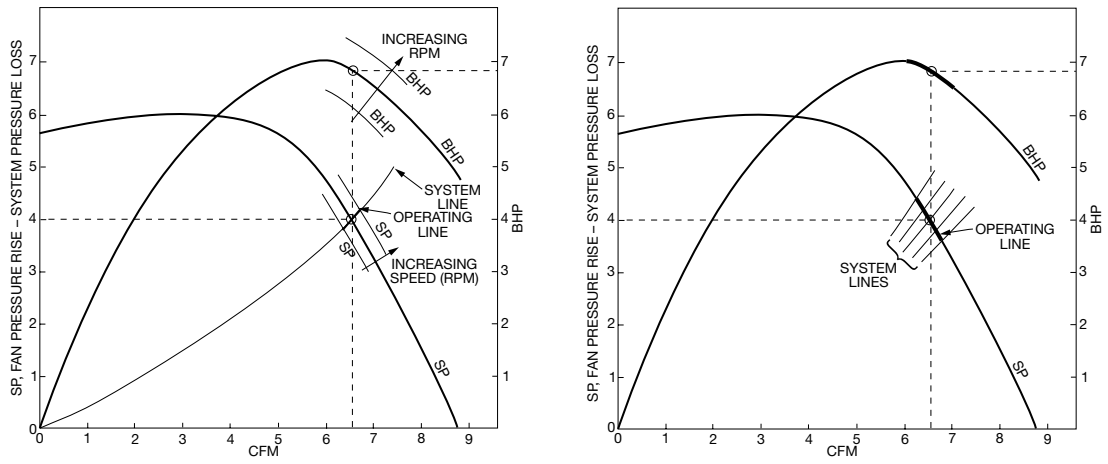

(a) Variable fan characteristics

(b) Variable system characteristics

Figure 2.7: Fan, system and power curves with variable characteristics [19]

By combining the fan and system controls in Figure 2.7, a fan/system control curve can be defined, as shown in Figure 2.8. This curve involves an *operating region*, which is a box defined by the operating lines along the fan and system curves. In other words, the box is the set of points of operation of the fan which can be obtained by adjusting the fan and/or system characteristics. The same thing applies for the power curve, which has its own region of operation.

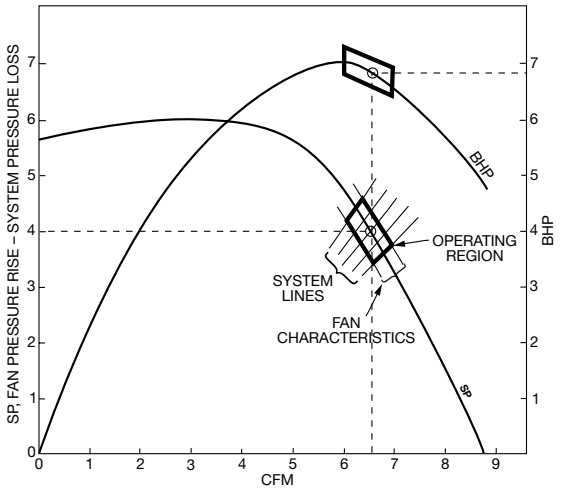

Figure 2.8: Fan, system and power control curves [19]

2.3.6 System losses

The curves for specific fans as in Section 2.3.5 are obtained from laboratory testing of fans in ideal conditions. When installing the fans for application however, the installation will differ from the laboratory setting, which will most likely produce sources of losses to the system. The losses may appear for different reasons but is usually connected with the duct system and other components.

2.3.7 Parallel operation

By having two identical fans operating parallel next to each other, the performance curves become slightly different from the case with one fan. Figure 2.9 shows the performance curves for the case with one and two fans in parallel operation in stable and unstable conditions. The curve A-A represents the performance curve for one fan and C-C represents the performance curve for two fans. The point CD is the operating point which is the limit between the stable and unstable region. All operating points to the right of CD belongs to the stable region and consequently, all the points to the left belongs to the unstable region. The instability can be explained by observing for instance the system curve E-E. The curve intersects the double-loop in the unstable region, which is showing all possible flow rates for a certain value of pressure. As shown in Figure 2.9, the system curve will intersect the loop twice, creating operating points CE and CE'. The fans will alternate between these two points and create a random pattern of behavior of the fans, which may produce undesirable side-effects such as noise, vibration and fatigue on the fans. Therefore, the fans should always operate in points to the right of the point CD in parallel operation. [16] [20]

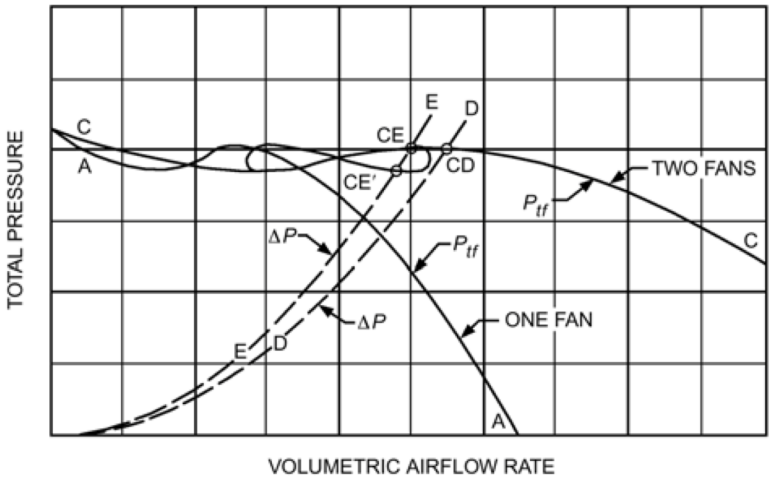

Figure 2.9: Performance curves for one and two fans [20]

3
Methodology

In this chapter, the methods used to obtain the wanted results are presented. It gives a detailed description of how the experiment was conducted, the geometry of the fan and AHU, generation of the mesh in the numerical simulations, the process of verification and validation and lastly a presentation of the modifications to the reference case.

3.1 Project structure

The flow chart of the project structure is shown in Figure 3.1. The first step is to prepare the simulation files in STAR-CCM+ by importing geometry, setting regions and boundary conditions, and generating the mesh. Parallel to this, a literature study is conducted in order to find appropriate mesh settings used in similar studies, to investigate other concepts used in attempts to improve fan efficiency and to find theory related to this study. A mesh study of the reference case is conducted in order to achieve mesh independence. This is made by starting with a fairly coarse mesh and refining regions which require finer mesh until the difference between the results of two mesh refinements are sufficiently small. The selected mesh is then used as reference for the new concepts, which are modifications to the AHU geometry, such as introducing a wall. CFD-simulations of the sought concepts and operating points are conducted, and finally the results from all simulations are analyzed and compared in order to draw relevant conclusions.

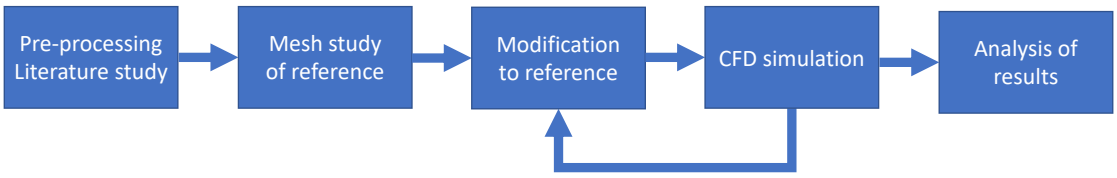

Figure 3.1: Flow chart of the main parts of the project

3.2 Experimental setup

The experimental testing of the AHU is carried out by Swegon at their testing facility in Kvänum prior to this study. The experimental setup is based on a scaled down version of Gold 80, one of the AHU currently being produced by Swegon. The test is conducted for nine variations of the AHU, where eight of them involve some kind of modification to the geometry which are of interest for investigation. Due to time limitations however, only two will be focused on in this study: the reference case and wall with the length 680 mm. For details about each of the variations, see Sections 3.3 and 3.4.1. Each of the tests are carried out at the same rotational speed of the fans and measurements at eleven different flow rates ranging from no flow to maximum flow possible. The same measuring equipment and methods are used for all test cases. The experimental setup is shown in Figure 3.2.

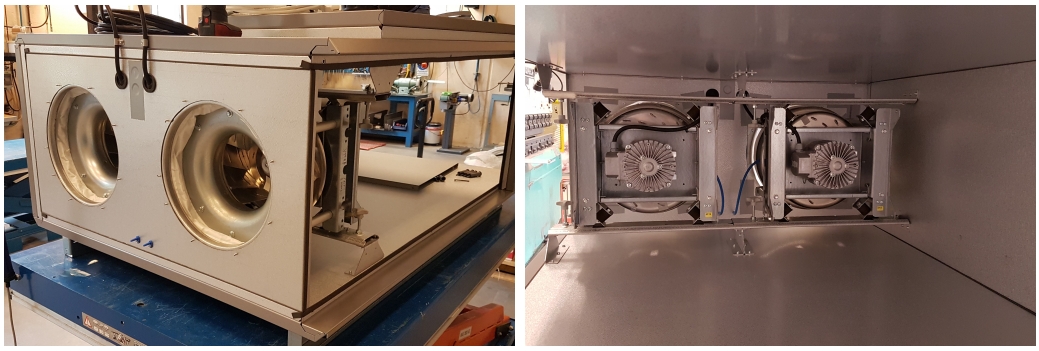

(a) Inlet region (b) Outlet region

Figure 3.2: Experimental setup for the reference case

3.3 Reference case

The reference case is the current design used by Swegon and will be used as the initial design from which the other concepts are developed from. This will also be used as a benchmark for comparison with the other concepts to determine the improvement value. The reference case is shown in Figure 3.3.

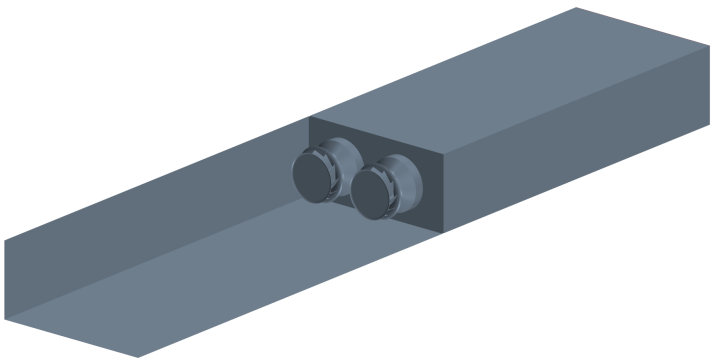

Figure 3.3: Isometric view of the reference case

3.3.1 Computational domain

The reference case of the AHU consists of a rectangular box with an inlet and outlet at each side of the box. In the middle of the box, the two fans are located parallel to each other. This is a simplified model compared to the real life AHU, where for instance the motors are removed, as it is decided that the inclusion of it will not have a major impact on the results, as well as to save computational power. Furthermore, the measurements are equal to the experimental setup, such that no scaling is necessary when analyzing the results. The geometry of the AHU and fan can be seen in Figures 3.4 and 3.5, and the measurements can be found in Table 3.1. The original case is expanded two meters in each direction along the flow axis in order to ensure fully developed flow at the inlet and to prevent backflow at the outlet.

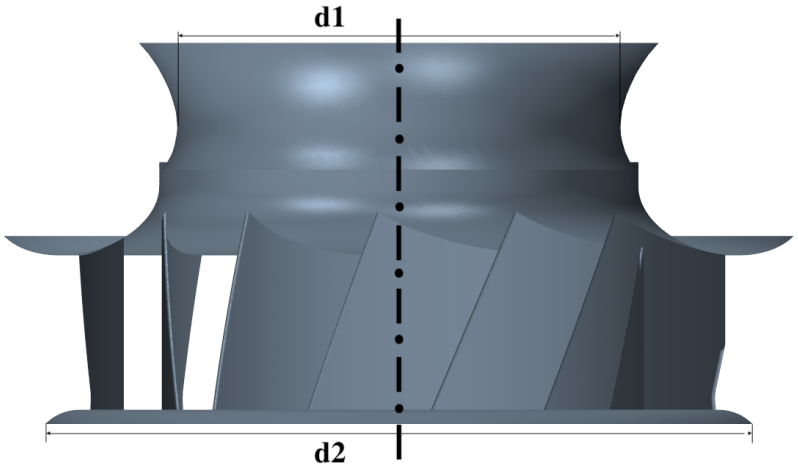

Figure 3.4: Cross-section of the fan with the parameters for inlet and outlet diameters

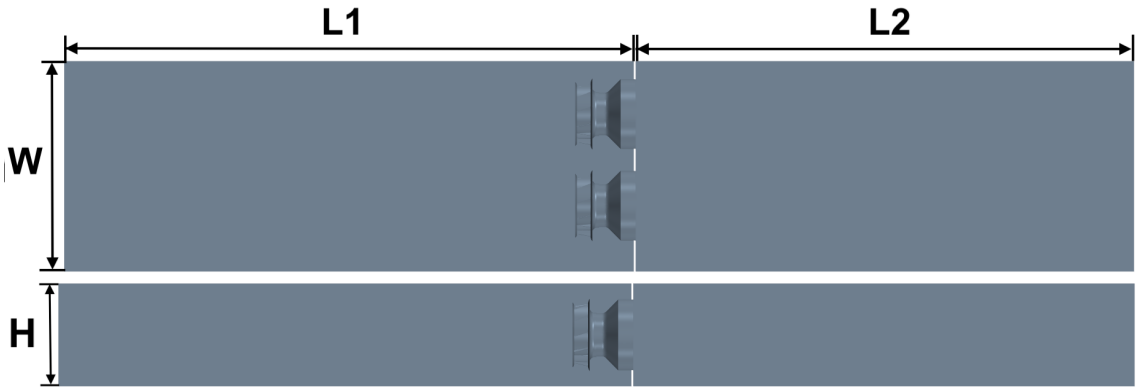

Figure 3.5: The computational domain seen from the top and side views and parameters of the lengths

Table 3.1: Parameters of the AHU and fan

Parameter	Value
d_1	0.22 m
d_2	0.36 m
L_1	3.20 m
L_2	2.80 m
W	1.19 m
H	0.40 m
Z	11

The computational domain is split into four regions: inlet, outlet and one for each fan. All region surfaces are set as wall except for the inlet and outlet boundary, which are set as velocity inlet and pressure outlet respectively. Additionally, there are three interfaces defined to connect the different regions. Interface 1 is the border between the inlet and fan regions, interface 2 is the border between the fan and outlet regions and interface 3 is the border of the small circular gap present very close to interface 1, again connecting the fan and outlet regions. The regions, boundaries and interfaces are shown in Figures 3.6 and 3.7, where red is inlet region, blue is outlet region and yellow is fan region.

Figure 3.6: The regions and boundaries defined in the computational domain

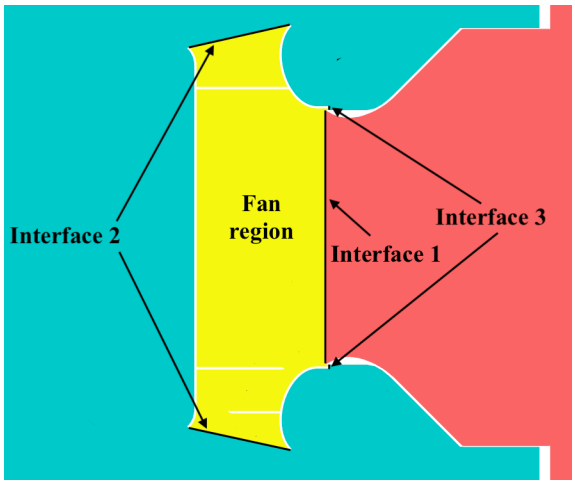

Figure 3.7: The regions and interfaces defined zoomed in at the fan region

3.3.2 Operating conditions

In this study, three different operating points will be simulated, see Table 3.2. These points will be obtained by setting a specific velocity flow input to the system in the simulations. The choice of these specific points is explained further under Section 4.1. The operating conditions are set by defining standard atmospheric pressure at the outlet and a constant rotational speed on the fans, see Table 3.3. The rotation of the fans is obtained by defining a moving reference frame for each of the fans. The reference frames are assigned to the fan regions, meaning that the fluid located inside those regions will rotate with the selected speed. Furthermore, the external parts of the shroud and backplate, which are located in the outlet region, are also assigned the rotational speed, as these parts are also rotating. Parameters which are not listed here are kept to their default values in STAR-CCM+.

Table 3.2: Operating points

Operating point	Volume flow [m^3/s]
1	0.90
2	1.07
3	1.26

Table 3.3: Operating conditions

Parameter	Value
Absolute pressure at outlet	101325 Pa
Fan rotational speed	2800 rpm

3.3.3 Models and solver settings

Steady state is chosen since the main interest is not in specific time steps of the simulation, as well as to save computational power. The flow is a single phase flow with the assumption of incompressible flow, due to the flow velocities being sufficiently low. In this study, the air is set to constant density of 1.225 kg/m^3. The flow is modelled with a segregated flow model, as it runs faster and is more suitable for incompressible flow than the coupled flow solver. The RANS model is chosen for calculating the equation of motion for the flow, while the moving reference frame is used to model the rotation of the fans. Lastly, the turbulence in the viscous regime is modelled using realizable two-layer k-ϵ model. The full list of models used is listed in Appendix A.

3.3.4 Mesh generation

A volume mesh is generated using polyhedral cells, which is an appropriate choice for a complex geometry. At the wall, the prism layer mesher is activated in order to capture the turbulent boundary layer correctly. The main idea with the core mesh is to accurately capture the flow characteristics, which is obtained by setting sufficiently small cell size where the flow is undergoing large changes, such as inside the fans. At the same time, the cell size should be set larger at regions where the flow is relatively stable and is not changing much, such as at the inlet. To enable a better control of the meshing, each region is assigned a separate mesh.

An important aspect of the mesh is the near wall cells. This has to be generated in such a way that makes the turbulence model valid and gives accurate results. Due to fine cell size needed for the fan parts, the choice is made to fully resolve the turbulent boundary layer and therefore aim for $y^+ = 1$, which is valid for the chosen turbulence model. This value is controlled by setting the near-wall prism layer thickness in STAR-CCM+, which is estimated as [21]:

$$\Delta s = \frac{y^+ \mu}{u_t \rho} \tag{3.1}$$

The choice of the resulting mesh used for the simulations is explained in Section 3.3.5. It contains 18.84 million cells and is the second finest mesh obtained from the mesh study. An overview of the mesh can be seen in Figures 3.8 - 3.11. In Figures 3.8 and 3.9, the cell size distribution is shown from the top view. It can be seen that the cell size is much smaller in the fan region and in the part of the outlet region surrounding the fans, as well as close to the walls. The same can be seen in the front view at the cross section of the fans, in Figure 3.10. The prism layer distribution for the inlet region is shown in Figure 3.11, where it can be seen that the transition from the last prism layer to the core mesh is smooth. The y^+ values at the blades and AHU walls are shown in Figure 3.12. It can be seen that the values for y^+ are within the range of 0-5 for all walls in the computational domain. Although the recommended aim is $y^+ = 1$, the acceptable range is the range of the viscous sublayer according to boundary layer theory, see Section 2.2.1. The number of prism layers for the surfaces are chosen between 12 and 18 depending on surface, which are obtained by finding a balance between acceptable y^+ values, smooth transition to core mesh, reasonable stretch factor of prism layer cells and recommended minimum value for this turbulence model. [22]

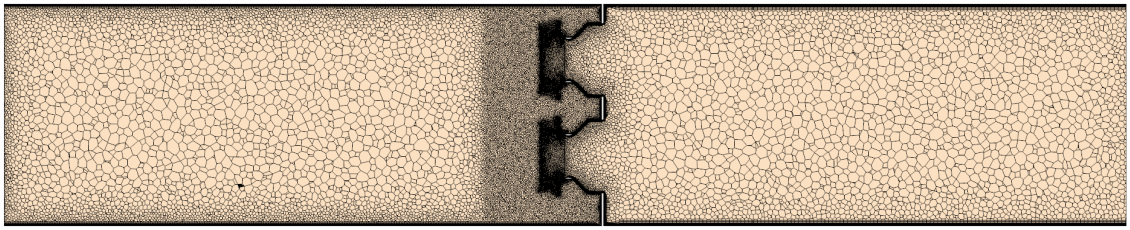

Figure 3.8: Top view of the mesh at the midplane of the domain

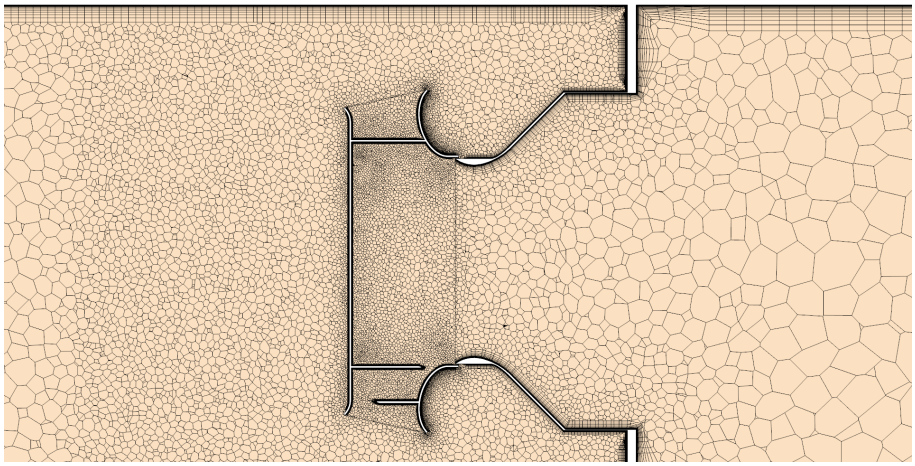

Figure 3.9: Top view of the mesh at the midplane of the domain, zoomed in at one fan

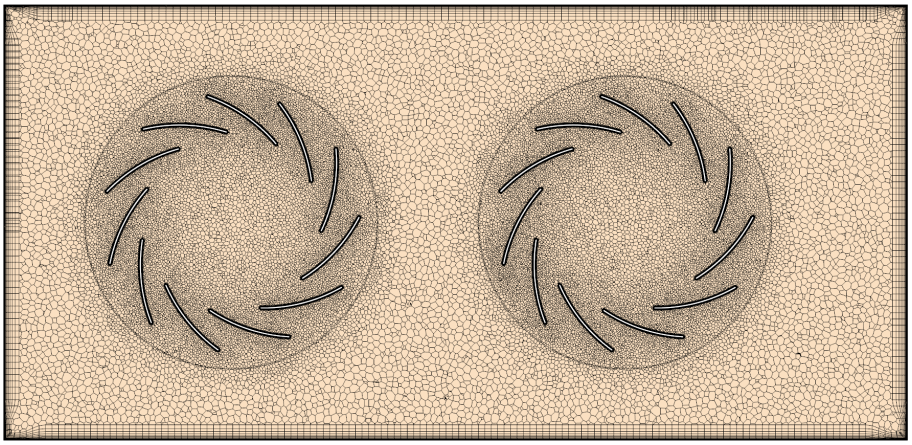

Figure 3.10: Front view of the mesh at the cross section in the middle of the fans

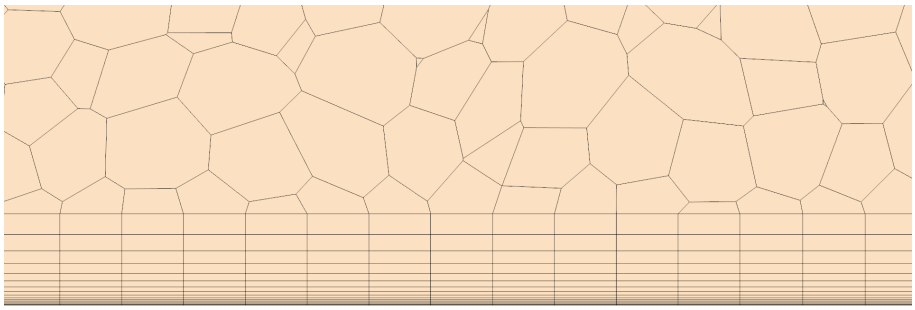

Figure 3.11: Top view of the prism layer distribution in the inlet region

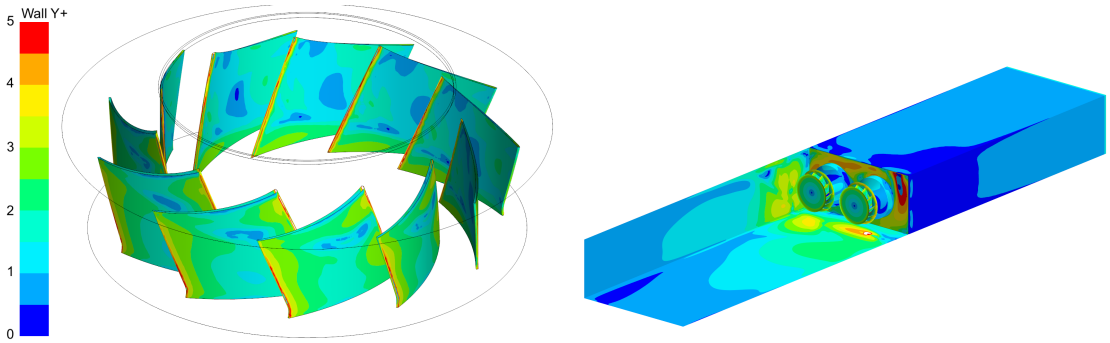

Figure 3.12: y^+ near the fan blades (left) and for the casing walls (right)

3.3.5 Verification and validation

To add credibility to the simulated results, a verification and validation (V&V) study is conducted. The purpose of the verification is to check if the simulations are solved correctly, and is performed by a mesh independence study. The validation on the other hand has a purpose to check if the correct simulations are solved, i.e. if the simulations match the real life. This is performed by comparing the results from simulation with experimental test results. Starting with the verification part, the mesh study is conducted for operating point 2 for the reference case. The criteria for convergence are partly based on recommendations from LEAP [23], which can be summarized as three conditions:

- Residuals values should be of acceptable values (typically below 10^{-4})
- Parameters of interest, inlet pressure and fan moment in this case, should reach a steady state solution.
- The fluctuations of the parameters of interest should be below 1 %.

When all three conditions are fulfilled and the simulation reaches a cyclic behavior of the measured parameters, the simulation is considered finished. The values of pressure and fan moment presented as results are obtained by averaging values of each iteration for the range of iterations during the last cycle. An example of a cycle for a finished simulation is shown in Figure 3.13 for the chosen mesh.

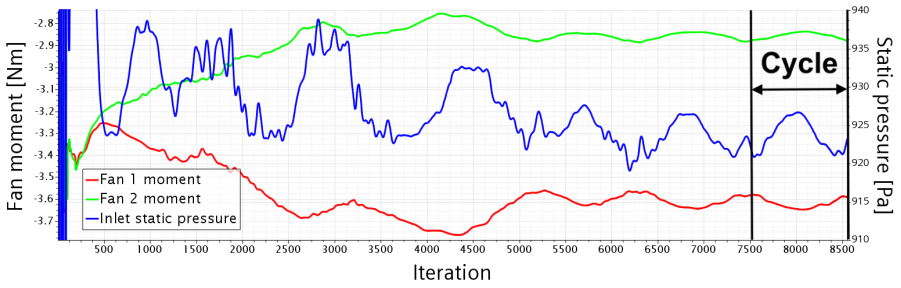

Figure 3.13: Fan moment and static pressure development for the chosen mesh with the definition of a cycle

Four different levels of mesh refinement are created named A, B, C, and D, where A is the coarsest and D is the finest mesh. Mesh A, the starting point of this study, is based on the mesh used in the previous study [8] in terms of cell count. The parameter used to check convergence between each refinement level is the static pressure. The aim for relative step size increase between each mesh level is around 1.0, where relative step size is defined as $h_i = (\frac{n}{n_0})$. The results from the mesh study are shown in Table 3.4 and Figure 3.14. The curves are obtained with the curve fitting tool in MATLAB, using the equation $a \cdot x^b + c$ to estimate the convergence. The error E is defined as $E = |\frac{p_1}{p_2}|$. It is found that E obtained between mesh C and D is below 1.0 %, which is decided to be an acceptable level of error, and therefore mesh C is chosen as mesh to run the simulations on. A full list of mesh settings is shown in Appendix B.

Table 3.4: Mesh study results

Mesh	Number of cells [M]	p_s [Pa]	h_i [-]	E [%]
A	6.1	977.2	1.0	3.3
B	12.4	945.9	2.1	2.4
C	18.8	924.1	3.1	0.3
D	24.1	926.5	4.0	-

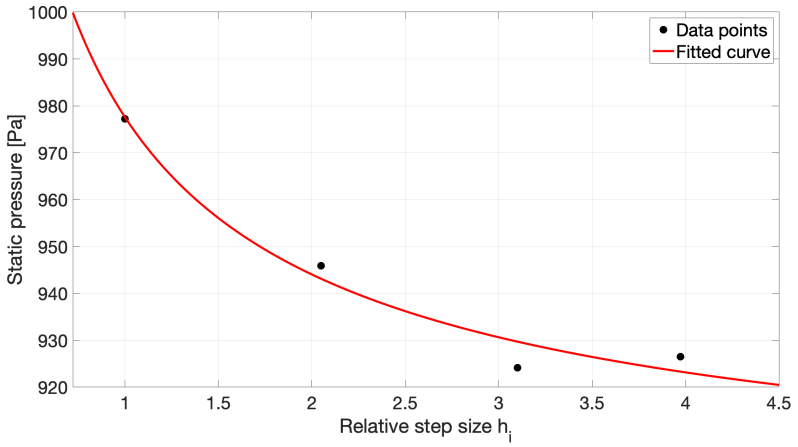

Figure 3.14: Static pressure convergence obtained by mesh study

The validation part of this study is conducted for mesh C, and for all three operating points chosen as defined in Table 3.2. In order to determine whether the results can be validated, the static pressure of the numerical simulations are compared to the one from experimental testing, and the error level is analyzed to make a decision. As seen in Table 3.5, the errors obtained are very high for a validation study, with 42.3 % being the lowest error for all operating points. Therefore the results cannot be validated with the experiments. This is discussed further under Section 5.4.

Table 3.5: Static pressure [Pa] for different operation points obtained from experimental testing compared to numerical simulations

Operating point	Volume flow [m^3/s]	Experiment	Simulation	Error [%]
1	0.90	657.7	936.1	42.3
2	1.07	572.6	924.9	61.5
3	1.26	443.4	926.2	108.9

3.4 Modified cases

This section presents and describes the three modifications that are compared to the reference case.

3.4.1 Concept I: Straight wall

The first modification is a straight wall in the outlet region which separates the flow produced by each fan. The main idea with this concept is to prevent the flow from each fan to collide with the other, i.e. try to reduce the turbulent kinetic energy in the region between the fans. The wall is located in the middle between both fans, has the same thickness as the casing (5 mm) and the length 0.68 m from the fan wall, which is the same length as the wall used in the experiment. The concept is shown in Figure 3.15.

Figure 3.15: Top view (left) and isometric view (right) of the AHU with the straight wall concept

3.4.2 Concept II: Tilted wall

The second modification is similar to the first concept. It includes a wall of same dimensions, but with the difference being that it is rotated 15.2° around the rotation axis of the fan. This angle is obtained by setting the connection point between the wall and case at the same horizontal distance from the center point as to the closest point of the fan. The idea with this concept compared to the straight wall is that the air flow will be more smooth at the corners. As the flow is rotating out of the fan, it will hit the wall with an angle of 105.2° instead of 90°. The concept is shown in Figure 3.16.

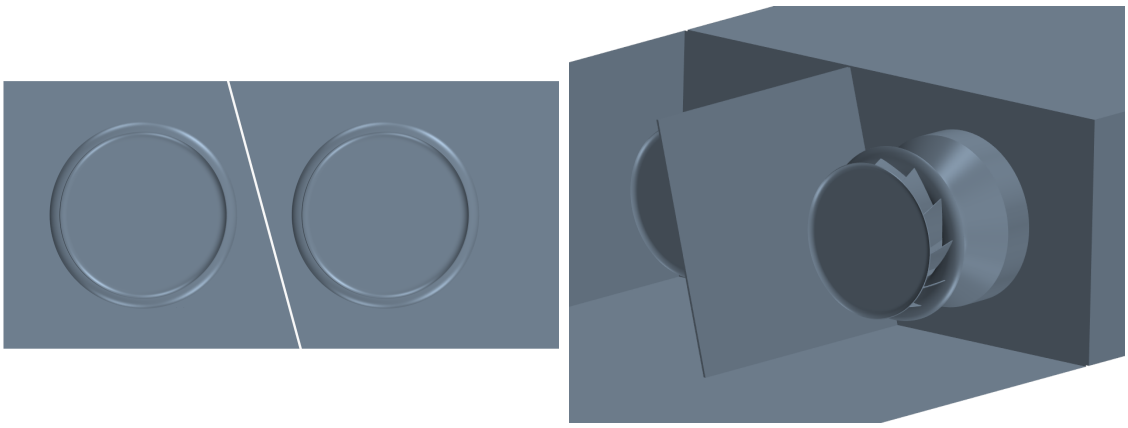

Figure 3.16: Front view (left) and isometric view (right) of the AHU with the tilted wall concept

3.4.3 Concept III: Curved wall

The third modification is similar to the straight wall, with the difference being that the wall is curved in the corners instead of being straight. The curves are designed as a quarter of a cylinder with radius of 200 mm, such that the center of the cylinder is located at the same distance from the center and top wall. The thinnest part of the wall, located at zero vertical distance from the fan center point, is set to be 5 mm, the same for which was used for the other two concepts. The length of the wall as well is kept the same as for the other wall concepts. The main idea with this concept is to investigate whether the added curvature compared to the straight wall concept will manage to help the flow by obtaining a more rotational behavior. The concept is shown in Figure 3.17.

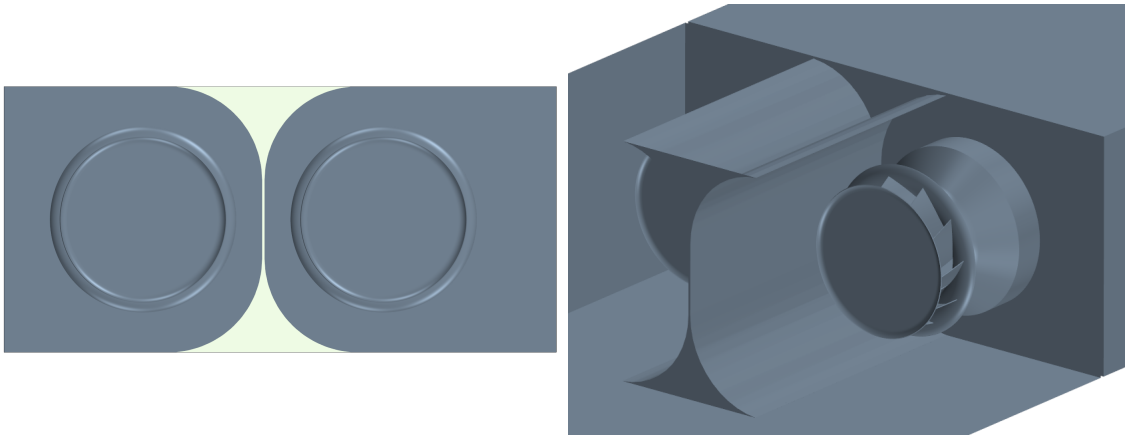

Figure 3.17: Front view (left) and isometric view (right) of the AHU with the curved wall concept

4
Results

In this chapter, the results from both experiments and numerical simulations are presented. In order to reach the goal of the project, a set of relevant physical quantities are chosen to analyze. These are chosen as velocity, turbulent kinetic energy, static pressure and fan efficiency.

4.1 Experimental test

The experiment is conducted for eleven different operating points, with volume flow ranging from 0 to around 1.7 m^3/s. The result from the tests is shown in Figure 4.1, where the blue graph shows the static pressure and the red graph shows the fan efficiency. The three points inside the ellipse are the points with the largest fan efficiency. As expected, these points are located in the recommended range located to the right of the maximum static pressure point, as explained in Section 2.3.5. Therefore, these points are selected as operating points for the simulations in this study.

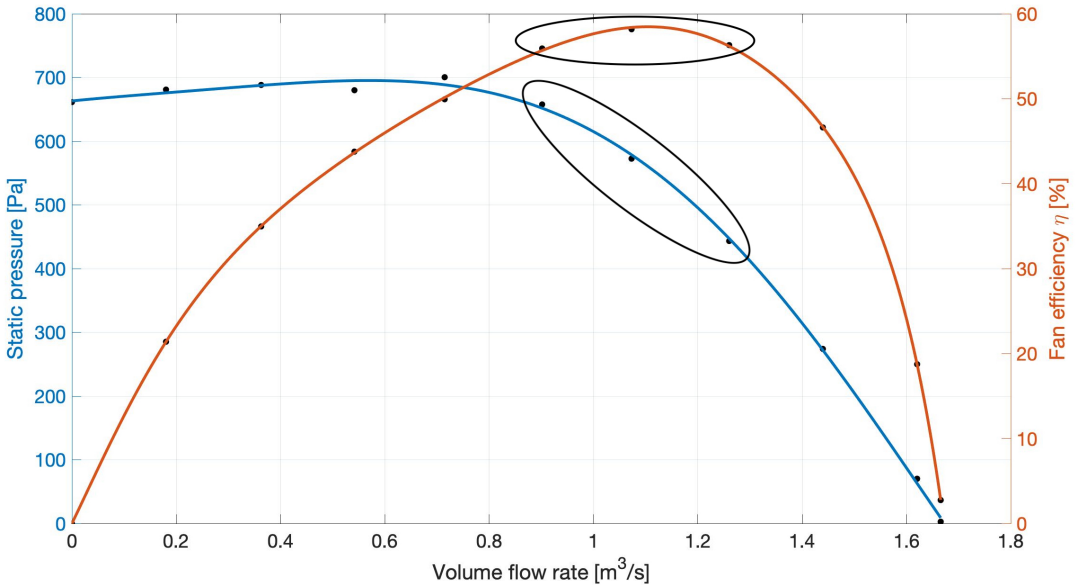

Figure 4.1: Static pressure and fan efficiency for a range of volume flows obtained from experimental testing of the reference case

The experimental results for the two test cases are analyzed for the three selected operating points. These results are summarized in Tables 4.1 and 4.2, and shown in Figures 4.2 and 4.3, for fan efficiency and static pressure respectively. The fitted curves are obtained by the curve fitting toolbox in MATLAB, where the fan efficiency is approximated as a ninth grade polynomial curve, whereas the static pressure is approximated as a fifth grade polynomial, as these produced the best match with the data points.

By including a wall, the fan efficiency is improved by approximately a half percentage point for all operating points compared to the reference case. The increase is 0.52 % for operating point 1, 0.48 % for operating point 2 and 0.56 % for operating point 3, meaning the increase for all operating points are similar to each other, with only a difference of 0.08 percentage point difference between maximum and minimum.

Table 4.1: Fan efficiency [%] at the three operating points for the two test cases (increase shown in brackets)

Operating point	Reference	Wall
1	55.92	56.44 (+0.52)
2	58.18	58.66 (+0.48)
3	56.31	56.87 (+0.56)

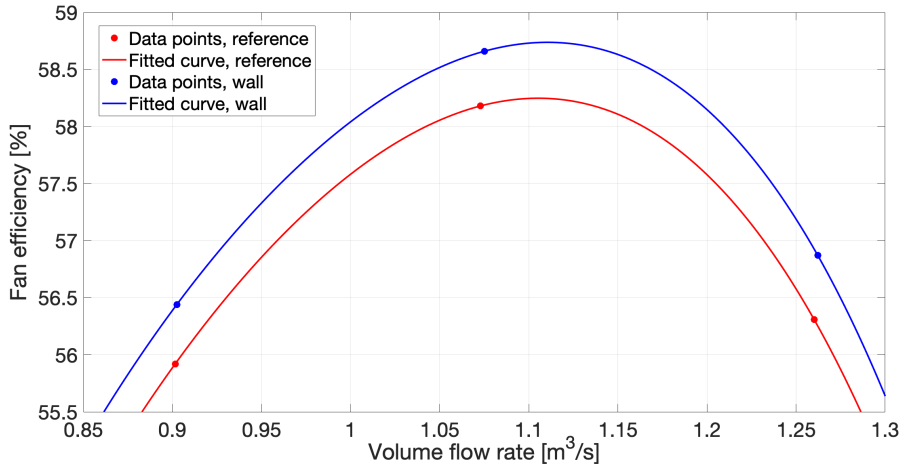

Figure 4.2: Fan efficiency [%] curve at the three operating points for the two test cases

Since the fan efficiency shows improvement for the wall concept compared to the reference, so should the static pressure. The wall produces an increase of 6.3 Pa for operating point 1 and 3.3 Pa for operating points 2 and 3. This means that operating points 2 and 3 have the same increase of static pressure, while it is almost the double for operating point 1.

Table 4.2: Static pressure [Pa] at the three operating points for the two test cases (increase shown in brackets)

Operating point	Reference	Wall
1	657.7	664.0 (+6.3)
2	572.6	575.9 (+3.3)
3	443.4	446.7 (+3.3)

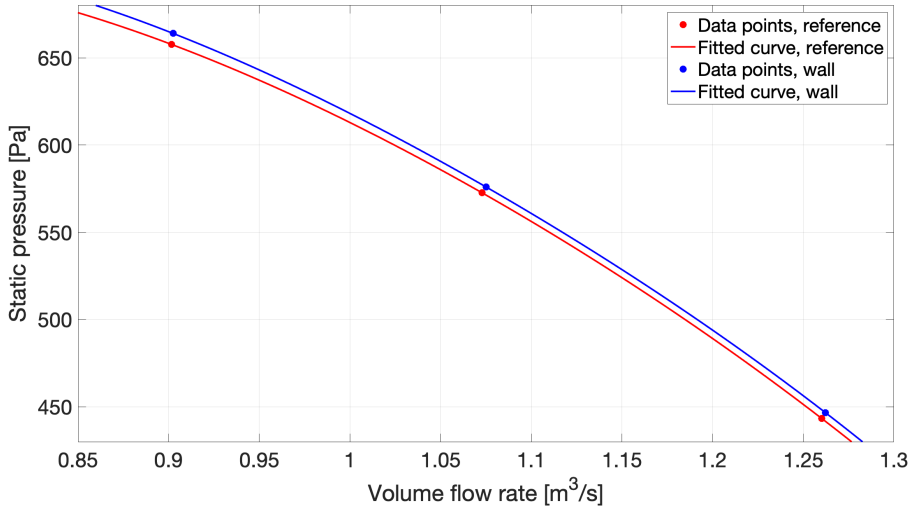

Figure 4.3: Static pressure [Pa] curve at the three operating points for the two test cases

4.2 Numerical results

In order to visualize the results obtained from the simulations, four planes in important parts of the domain are created. Plane 1 is the cross section of both the fans in yz-plane. Plane 2 is located in the same plane but offsetted by 0.2 m downstream from the backplate. Plane 3 is the cross section in the middle of fan 2 in the xz-plane. Lastly, plane 4 is the cross section in the middle of both fans in the xy-plane. The plane sections and their names are shown in Figure 4.4.

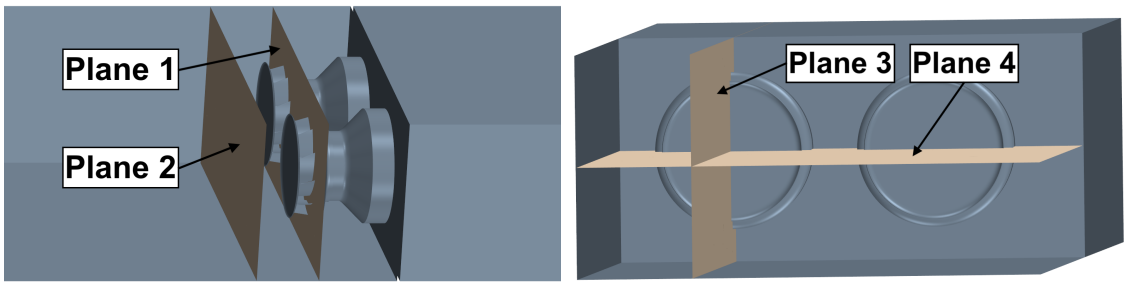

Figure 4.4: Plane sections used for analysis of results with corresponding names

4.2.1 Velocity streamlines

In order to find potential sources of pressure loss and other important regions in the outlet side of the AHU, the velocity streamlines are analyzed. By observing the front view of plane 1, the wanted profile of the flow is a circular pattern where the velocity is kept as close to the exit velocity from the fan as possible. In this plane, this behavior can be found for all cases in the region close to the outer walls. However, when observing the region between the fans, it can clearly be seen that for the reference case, the airflow is irregular and shows a large velocity drop compared to the modifications. The wall concepts are handling this much better, and especially the curved wall shows the best looking airflow in this plane, with no large velocity drops or irregularities.

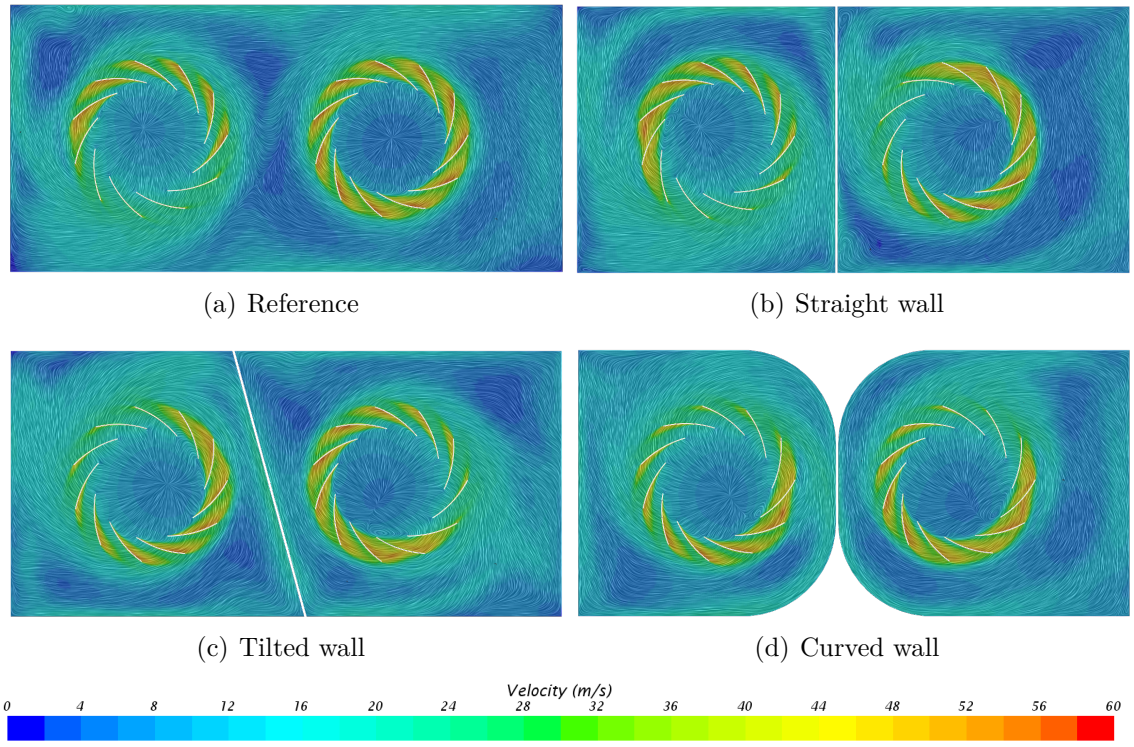

(a) Reference (b) Straight wall

(c) Tilted wall (d) Curved wall

Figure 4.5: Velocity streamlines for the different concepts for operating point 2 in plane 1

When analyzing the flow in plane 2, which is located further downstream than plane 1, the same characteristics of the streamlines are wanted as for plane 1. It can be seen that the behavior is similar to plane 1, all cases show good flow at the outer walls, while the modifications produce better flow between the fans compared to the reference. Some differences can be noticed however. First of all, the curved wall shows the best flow at both the inner and outer wall, with large velocity magnitude and low velocity drop at the corners compared to the other cases. Between the straight wall and the tilted wall there is no huge difference except at the inner wall, where the velocity is kept large along a longer distance for the tilted wall.

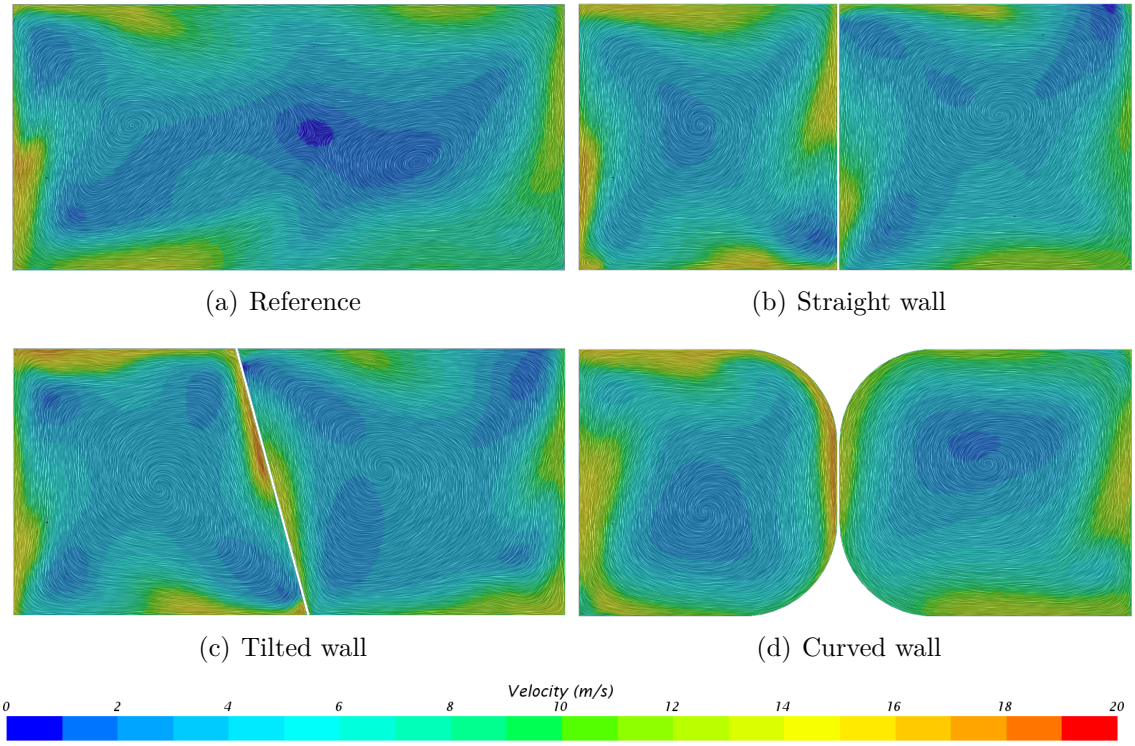

(a) Reference

(b) Straight wall

(c) Tilted wall

(d) Curved wall

Figure 4.6: Velocity streamlines for the different concepts for operating point 2 in plane 2

For the side view in plane 3, the ideal behavior of the airflow is out from the fan blades and straight towards the outlet without causing any swirls or rotations. For a couple of reasons this is not possible to achieve, such as the design of the AHU. But it is possible to minimize the effect of swirls and force the flow to be close to the ideal case. By observing the flow along the outer wall, is it found that the curved wall performs well, as the velocity manages to keep a relatively large and constant magnitude. The streamlines are found to be fairly straight with few swirls, which also hold true for the tilted wall, which however experiences a decrease in velocity towards the outlet. For the straight wall, the velocity keeps similar magnitude as the tilted wall, but for this case the streamlines start to lose its straight pattern towards the outlet. Finally, for the reference, the streamlines do not look close to ideal, which is due to the strong swirling in this design. The flow in front of the backplate of the fans is also important. The modifications all have large regions of low velocity compared to the reference. Especially the curved wall has the largest region, while the straight and curved wall have similar.

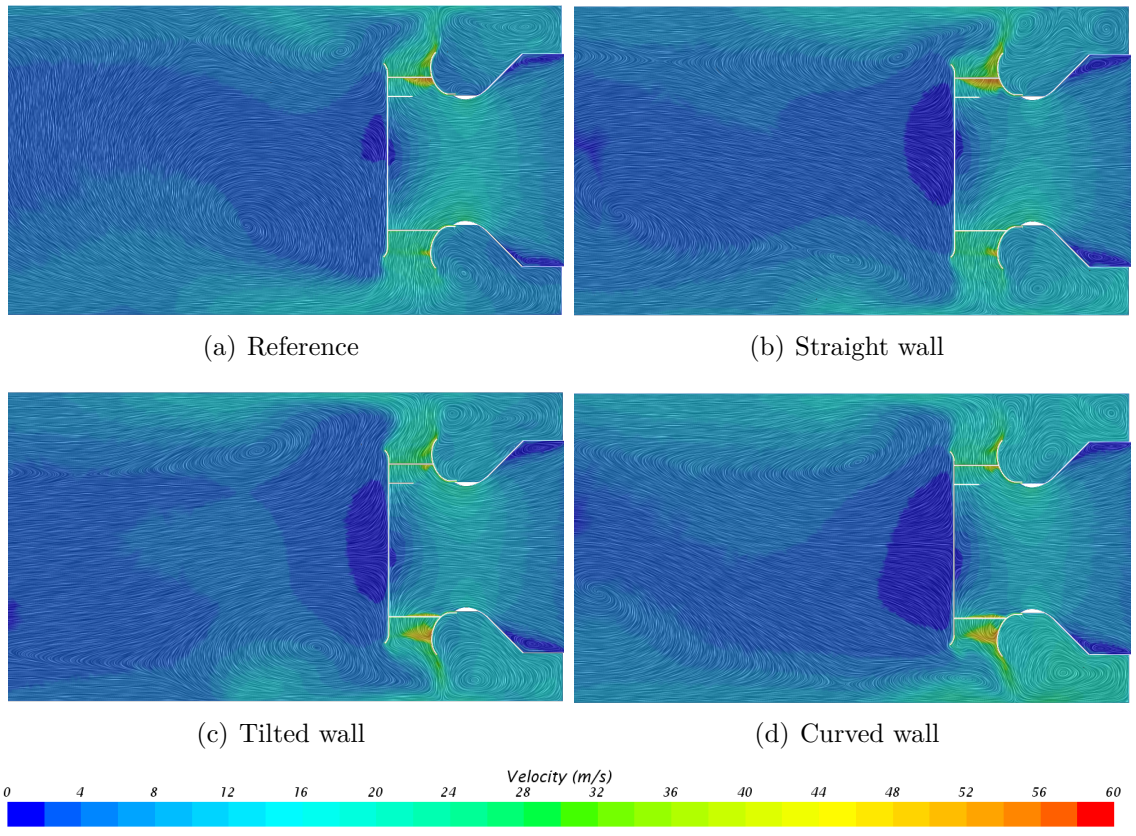

(a) Reference

(b) Straight wall

(c) Tilted wall

(d) Curved wall

Figure 4.7: Velocity streamlines for the different concepts for operating point 2 in plane 3

For the plane showing the top view, the same ideal conditions are wanted as for plane 3, including a behavior at the inner wall as similar as possible to the outer wall. Since the reference does not have an inner wall, the velocity streamlines between the fans will collide, creating a chaotic region with swirls and low velocity further downstream. Meanwhile, for the modifications, the flow behaves much better between the fans. The velocity magnitude is kept large along the wall and is kept for the entire length of the wall. Additionally, the flow close to the outer side walls is found to be similar between all cases, however the straight wall and tilted wall falls short due to small regions in the bottom part with very low velocity, which is handled better in both the reference and the curved wall.

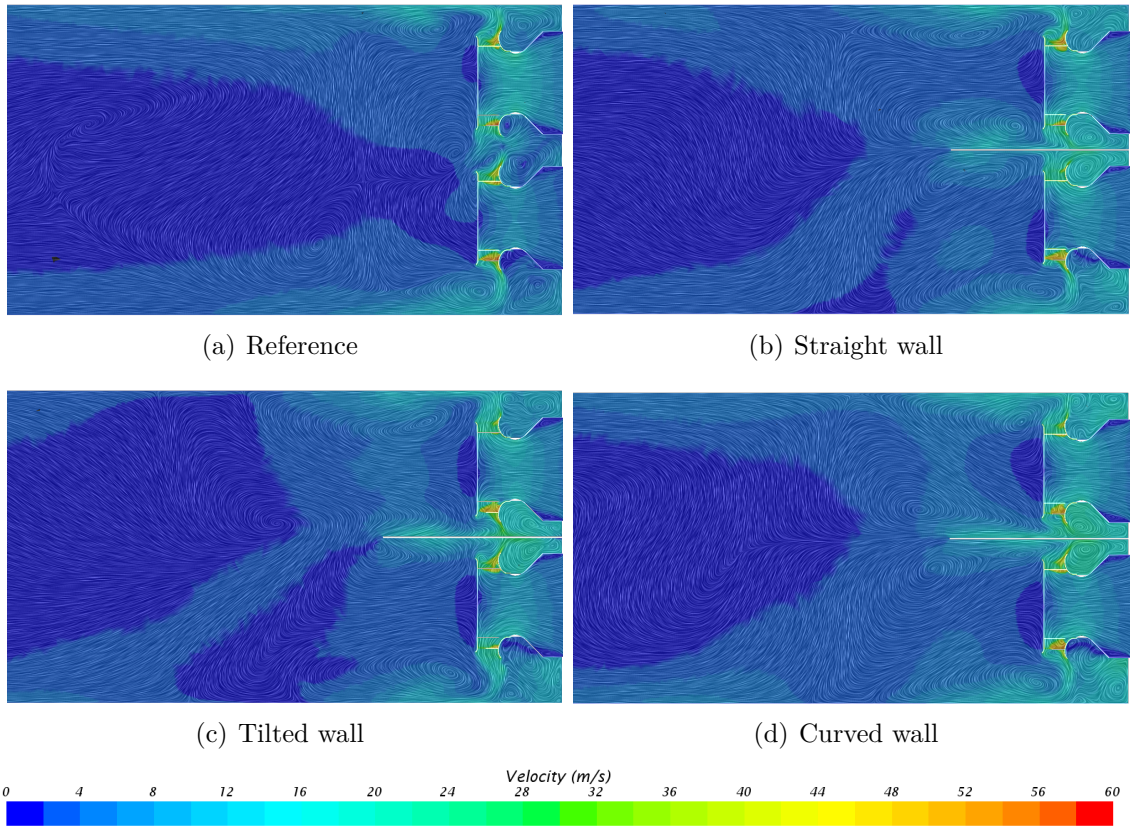

(a) Reference

(b) Straight wall

(c) Tilted wall

(d) Curved wall

Figure 4.8: Velocity streamlines for the different concepts for operating point 2 in plane 4

4.2.2 Turbulent kinetic energy

The other parameter analyzed in contour plots is the turbulence kinetic energy (TKE). It is an important property to observe because it gives an indication to regions where turbulence is generated, which might be indications of pressure loss regions. By observing the front view of plane 1, it can clearly be seen that the region between the fans gives relatively large values of TKE when compared to the modifications. This is, as for the velocity streamlines, explained with the fact that the airflow out from the fans collide and create a region of turbulence. Comparing the modifications, it is found that the performance with regards to TKE is similar, with the straight wall showing the best results at the middle wall, followed by the curved wall and lastly the tilted wall.

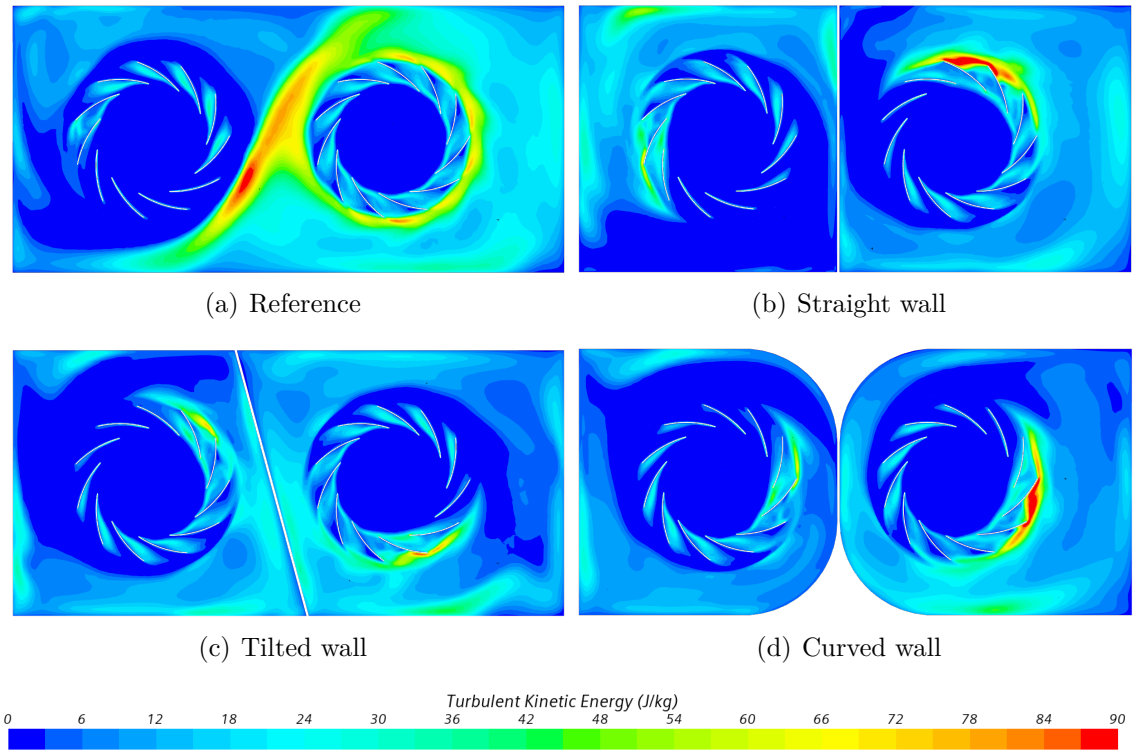

(a) Reference (b) Straight wall

(c) Tilted wall (d) Curved wall

Figure 4.9: Turbulent kinetic energy for the different concepts for operating point 2 in plane 1

Moving slightly downstream to plane 2, it is found that the values of TKE are lower of magnitude for all concepts when compared to plane 1. In this plane, the region of large TKE is located in the middle section along each wall, including the middle wall for the modifications, which is visualized as the green-yellow regions in Figure 4.10. Exceptions to these observations are found for the curved wall, which has smaller regions of low TKE below the left fan and above the right fan, and for the reference, which has a region of relatively large TKE below the left fan.

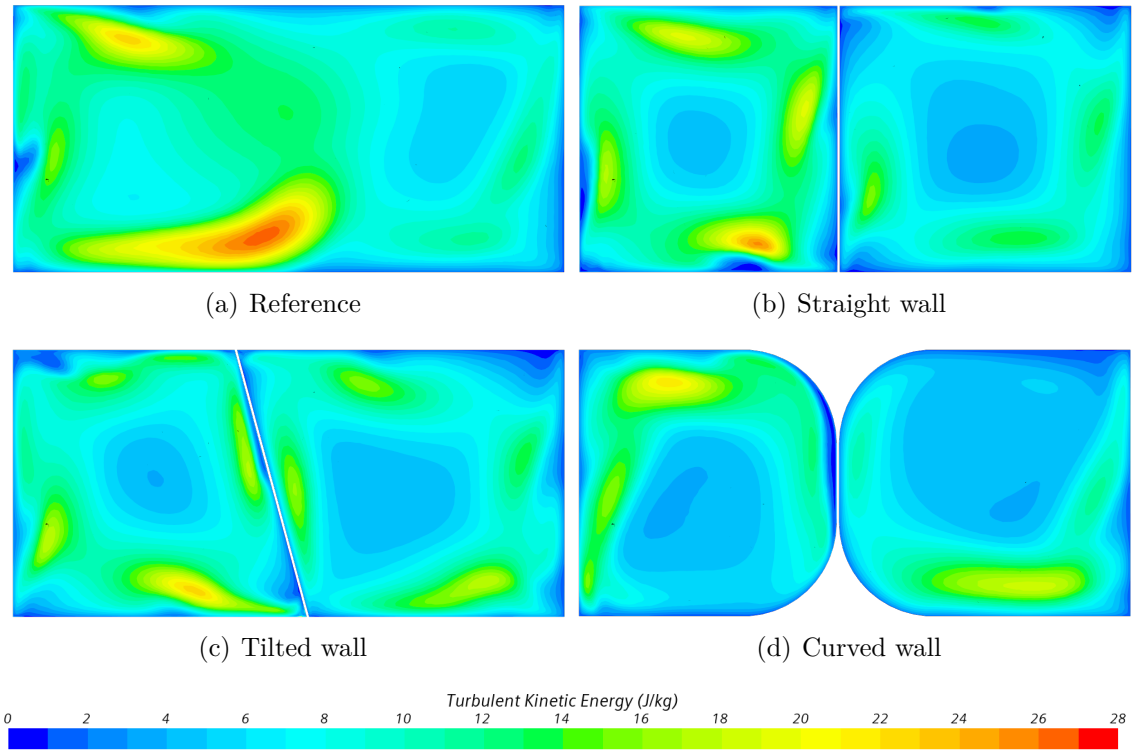

(a) Reference

(b) Straight wall

(c) Tilted wall

(d) Curved wall

Figure 4.10: Turbulent kinetic energy for the different concepts for operating point 2 in plane 2

The side view of the left fan is shown in Figure 4.11. As the flow exits the fan, TKE is increased close to the outer walls of the casing, visualized as green regions above and below the fan. These regions correspond to regions where swirls are present in the velocity plots in Figure 4.7. Hence, the swirls act as sources of turbulence. All cases show similar results in these regions with locally smaller regions of larger or smaller magnitudes of TKE. The flow differences in the region in front of the backplate is another finding. The modifications all have lower TKE in this region compared to the reference.

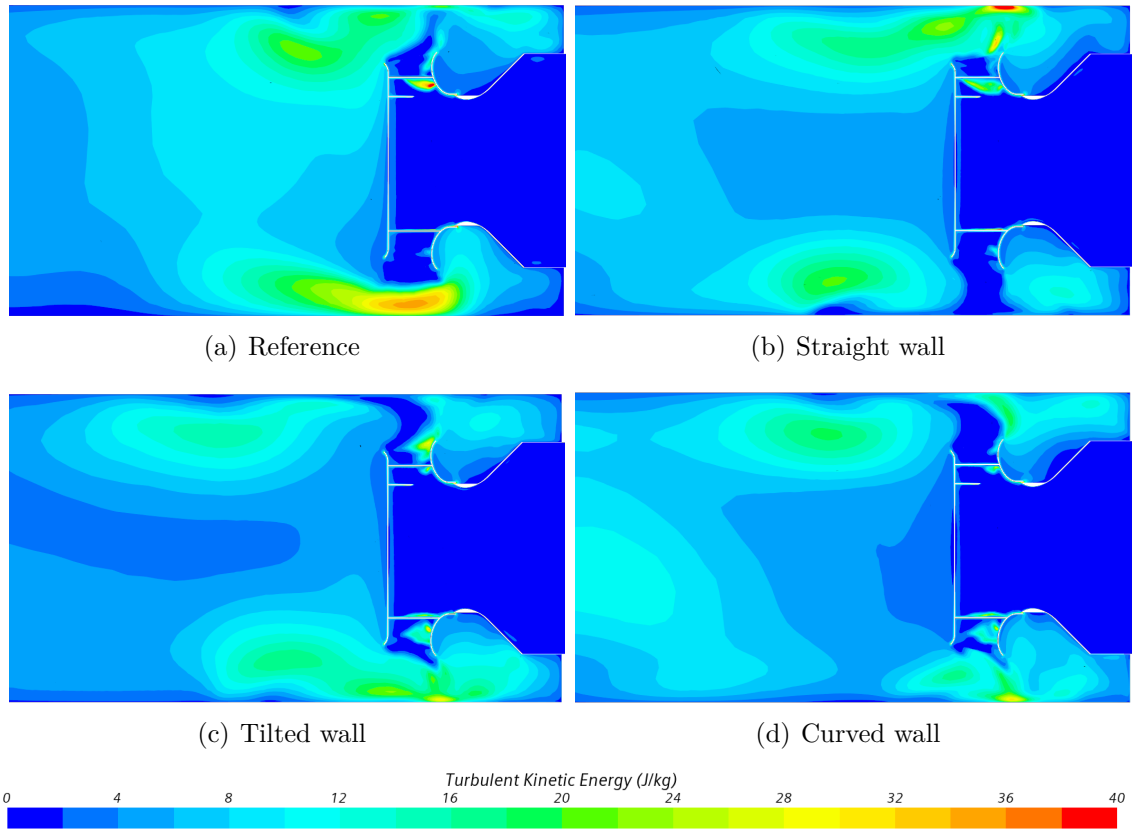

(a) Reference (b) Straight wall

(c) Tilted wall (d) Curved wall

Figure 4.11: Turbulent kinetic energy for the different concepts for operating point 2 in plane 3

Observing the top view of plane 4 in Figure 4.12, some of the observations from the other planes can be confirmed. Here it again becomes clear that the region between the fans produce very large amount of TKE, which is indicated as a region of red color with green/cyan surrounding in Figure 4.12(a). It is worth noting that the range for this figure is the largest and that the regions of high turbulence have larger magnitude of TKE compared to the other figures in this section. As for the region in front of the fans, it can similarly as in Figure 4.11 be seen that the modifications handle the turbulence generation better than the reference, especially the curved wall.

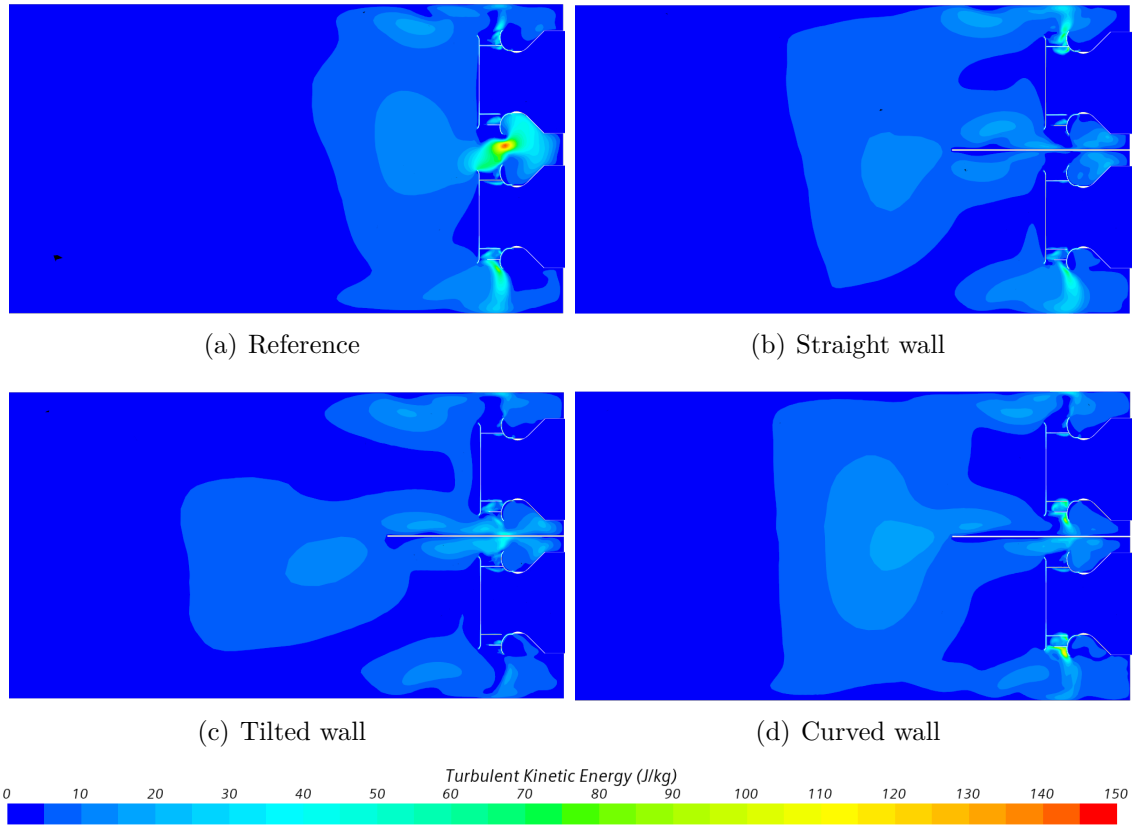

(a) Reference

(b) Straight wall

(c) Tilted wall

(d) Curved wall

Figure 4.12: Turbulent kinetic energy for the different concepts for operating point 2 in plane 4

4.2.3 Static pressure

The static pressure is strongly related to the fan efficiency and is therefore an important parameter to observe. By keeping the volume flow constant and finding a pressure increase when comparing the different concepts, one can expect the fan efficiency to increase as well. The static pressure obtained from the simulations are defined as the average pressure at the inlet boundary surface. The static pressure values for the different cases are shown in Table 4.3 and in Figure 4.13.

In the table it can be seen that all the modifications show an increase in pressure to varying degree when compared to the reference. For operating point 2, the increase is as much as 29.2 Pa for the straight wall, which is a significant increase compared to the experiment, which gave 3.3 Pa for the same operating point.

Table 4.3: Comparison of static pressure [Pa] between the different concepts for the three operation points

Operating point	Ref.	Straight wall	Tilted wall	Curved wall
1	936.1	946.9	943.9	949.6
2	924.1	953.3	951.5	944.1
3	926.2	946.8	948.3	938.2

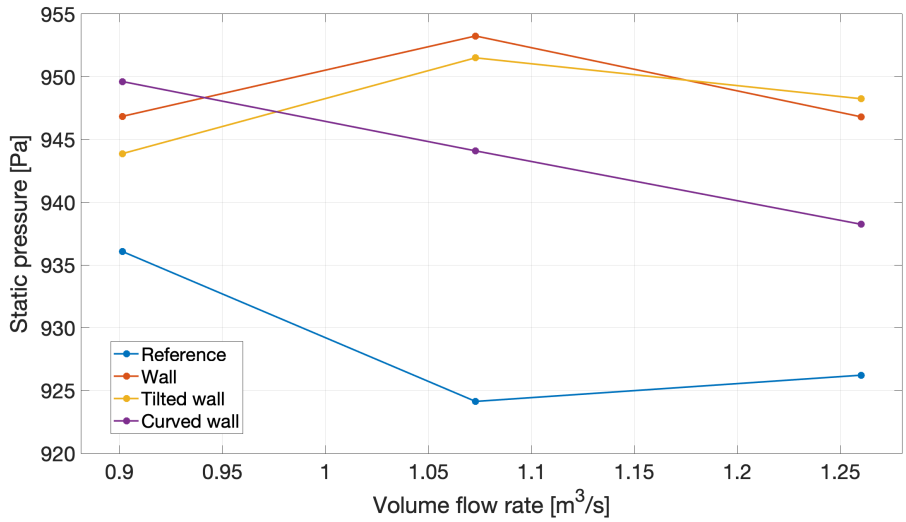

Figure 4.13: Comparison of static pressure [Pa] between the different concepts for the three operation points

4.2.4 Fan efficiency

As with the static pressure, the fan efficiency values are obtained for each case, as shown in Table 4.4 and in Figure 4.14. The values are obtained by inserting each parameter from the simulations into Equation 2.10 in Section 2.3.4. All modifications shown significant increase of efficiency and follow a similar line parallel to the line of the reference case. For operating point 1 the curved wall is slightly larger than the other modifications, while for operating point 3 the tilted wall performs slightly better.

Table 4.4: Comparison of fan efficiency [%] between the different concepts for the three operation points

Operating point	Ref.	Straight wall	Tilted wall	Curved wall
1	47.32	48.93	48.86	49.35
2	52.31	54.39	54.39	54.36
3	57.59	59.19	59.35	59.20

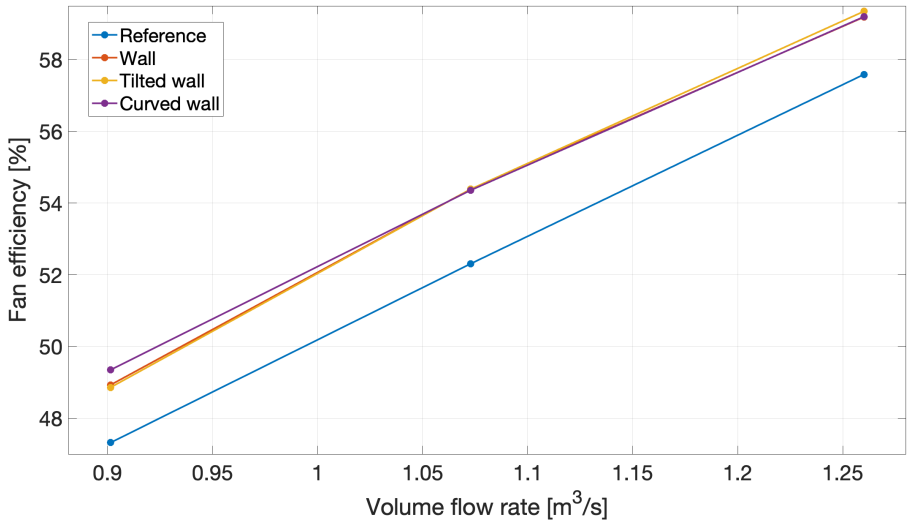

Figure 4.14: Comparison of fan efficiency [%] between the different concepts for the three operation points

4.2.5 Range of improvement

In order to determine the potential improvement of each concept, all three operating points are taken into account to create the range of improvement in terms of fan efficiency. From Table 4.5 and Figure 4.15 it can be seen that the wall concepts have a similar range from around 1.54 up to 2.08 %. The curved wall has the smallest range of improvement, while the tilted has the largest range and at the same time both the minimum and maximum improvement value out of all modifications.

Table 4.5: Improvement of fan efficiency [%] for the different concepts compared to the reference case

Operating point	Straight wall	Tilted wall	Curved wall
1	1.61	1.54	2.03
2	2.08	2.08	2.05
3	1.60	1.82	1.61
Range	1.60 - 2.08	1.54 - 2.08	1.61 - 2.05

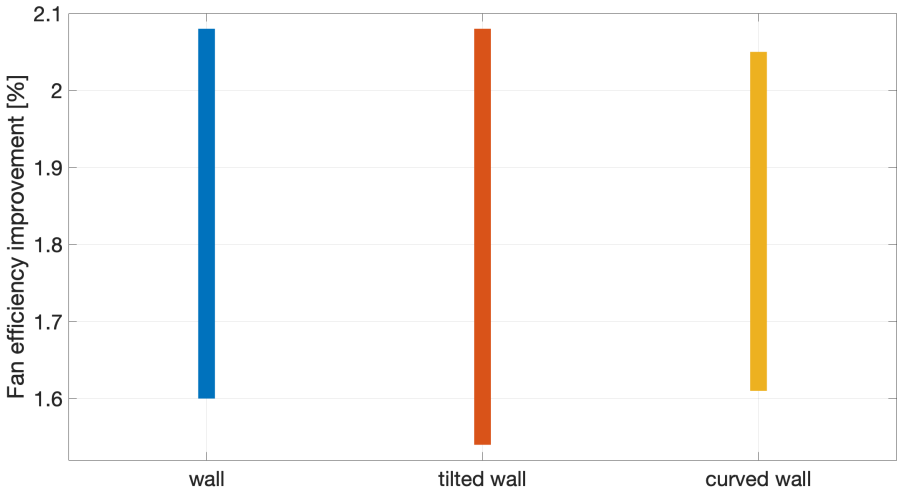

Figure 4.15: Range of improvement in terms of fan efficiency compared to the reference case for each modification

5
Discussion

In this chapter, the obtained results are discussed and analyzed in order to draw conclusions.

5.1 Regions of interest

By observing the plots of velocity streamlines and turbulent kinetic energy, it can be found that there are a couple of interesting regions which are important to investigate. The first region is the interaction region located between the fans. This is the main difference from the single fan AHU because in this case, the flow coming from each fan will collide and create turbulence, which in turn produce a pressure loss. This collision is evident in Figure 4.12, where it is shown as a red point for the reference case, representing large values of turbulence. It becomes clear that by separating the two flows, for instance with some kind of wall, the interaction region does not act as a source of pressure loss anymore. All modifications manage to handle this region well, but the best performing based on the results is the curved wall, probably due to the smooth transition when rounding the corner, compared to the straight wall and tilted wall.

The second region of interest is the recirculation region in front of the backplate of each fan. Since the fans are radial, the flow will obtain a rotational behavior, which creates swirls close to the outer walls. These swirls cause the flow to recirculate and move in the opposite direction at the backplate, which can be seen in Figures 4.7 and 4.8. This behavior is undesirable, as it acts as a source of turbulence, as seen in Figure 4.11. By including a wall, it reduces the recirculation, as the wall helps the flow reach a desirable pattern in the interaction region and a short distance further downstream. This is based on the lower velocity magnitude observed for the modifications compared to the reference. The modification handling this region best was found to be the curved wall, as it contained the lowest magnitudes of velocity and turbulent kinetic energy out of all modifications.

The third region observed is the outer walls region located along the sides of the AHU casing. It is mentioned in Section 4.2.1 that a straight flow in this region is ideal. The reason for this is because it will reduce the effect of the swirls created close to those walls, which in turn will improve the flow in both the recirculation and interaction region. For instance, by observing the velocity streamlines in Figure 4.7, it can be seen that the swirls for the reference are large in size, which is causing the relatively large and unwanted velocity at the backplate. By forcing the swirls close to the outer wall and by keeping it small, as it is for the curved wall, the negative effects are reduced in the other regions.

5.2 Comparison between concepts

The magnitude of the impact of each region must be determined by comparing the obtained static pressure and fan efficiency for each case. Starting with the static pressure for operating point 1, the curved wall performs best, as it achieves an increase of more than 13 Pa compared to the reference case. Followed by the curved wall are the straight wall and tilted wall modifications, which produce similar results, around 7-10 Pa more than the reference. Looking at operating point 2, the curved wall decreases in pressure from operating point 1 while the straight wall and tilted wall increases, meaning that those two overtake the curved wall. The straight wall and tilted wall are have an increase of around 27-29 Pa and the curved wall of around 20 Pa compared to the reference. Lastly, looking at operating point 3, the straight wall and the tiled wall concepts again produce very similar pressure, around 20-22 Pa more than the reference, and the curved wall around 12 Pa more than the reference. A similar analysis is conducted for the fan efficiency. However, the pattern is more clear for this, as the slopes are very similar to each other, giving an almost parallel behavior of the slopes. Exceptions to this behavior can be found for operating point 1, where the curved wall has around 0.42-0.49 % more than the straight wall and tilted wall, and for operating point 3, where the tilted wall has around 0.15 % more than the straight wall and curved wall.

5.3 Comparison between methods

In addition to comparing the modifications, it is also of interest to compare the experimental test data to the numerical simulations. Interestingly, the comparison between static pressure and fan efficiency show quite a large difference. The static pressure, as explained in Section 3.3.5, differs significantly between the experiments and simulations, with errors between 42.3 and 108.9 %. The decrease is also found to be much bigger in the experiment compared to the simulations. The drop in the reference case from operating point 1 to 3 is 214.3 Pa for the experiment, compared to 9.9 Pa for the simulation. Looking at the fan efficiency though, the errors are not as large as for the static pressure. For instance, by analyzing the reference case, it is found that the errors are 15.4 % for operating point 1, 10.1 % for operating point 2 and 2.3 % for operating point 3. These error levels are more acceptable than those obtained for the static pressure.

Despite the error levels, it is of interest to compare the improvement between the concepts for each method. The concepts in comparison will be the two that are present in the experimental testing, namely the reference and the straight wall. The comparison is summarized in Figure 5.1. A couple of general observation points can be made for both parameters:

- The simulations are overpredicting the parameters compared to the experiments.
- The wall outperforms the reference both in the simulations and the experiments.

In Figure 5.1, a comparison is shown between both methods for the improvement value of the wall compared to the reference. Starting with fan efficiency, the difference between the methods is fairly similar for all operating points, with the largest deviation of 1.60 percentage points at operating point 2 and lowest deviation of 1.04 percentage points at operating point 3. The static pressure on the other hand, varies hugely between the different operating points. The lowest deviation of 4.5 Pa is found at operating point 1, while the largest deviation of 25.8 Pa is found at operating point 2.

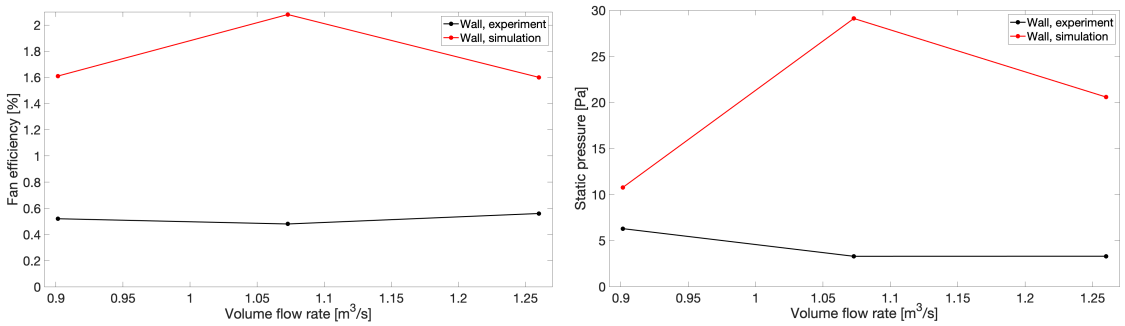

Figure 5.1: Comparison between experimental test and numerical simulation of the improvement of fan efficiency (left) and static pressure (right) by using the wall compared to the reference for all three operating points

5.4 Models selection

When analyzing the results, it is important to take into account which models are used in the simulations, as the selection makes a great impact on the results. The biggest impact is most likely due to the choice of running steady state, which provides a time-averaged solution. If instead a transient solver was used, the solution would be time given for each time step, giving a more accurate picture of the flow. However, due to resource limitation, the steady state solver was the only option. This may be a reason to why the values of the static pressure is overpredicted in the numerical simulations compared to the experiments. The steady solver may simply not be able to accurately obtain the real life behavior of the flow for the parallel fan operation. Therefore, this might be a source to why the numerical results could not be validated in the V&V study.

Strongly connected to the choice of the steady state solver is the choice of using the moving reference frame, as it works well with time-averaged solvers. There are however alternatives to the moving reference frame, such as the rigid body motion. This method is more suitable with transient solvers as it uses a slip-mesh, which rotates the mesh cells in the region which is rotating. [24] This method would probably produce more accurate results, but as for the time solver, this is not possible due to resource limits.

Another factor which may have a big impact on the results is the choice of turbulence model. Trying various turbulence models and comparing the performance was left out of the project, as it is out of the scope of the study. However, several simulations were conducted with the k-ω SST (Shear Stress Transport) model during the V&V study to check whether the results might be better for validation compared to the results with the k-ϵ model. It was found that the results did not differ much, and was therefore decided that the turbulence model should be kept as initially chosen.

5.5 Environmental impact

One of the main reasons to improve the fan efficiency is to lower the environmental impact by being able to keep the AHU performance, while lowering the power needed for the motors to rotate the fans. Assuming that a fan requires the motor to run at 1 kW to obtain the conditions of operating point 2 for the reference case, it means that the AHU requires 2 kW with an efficiency of 52.31 %. Inserting the same conditions but for the curved wall for instance, with an efficiency of 54.36 %, the power required turns out to be 1.925 kW, which is a decrease of 75 W. At first glance this may seem like a small improvement, but if this modification was implemented into every one of the 120000 installed Gold units in the world [25], the energy saved would add up to 9 MW. This is approximately the amount of energy generated by three average on-shore wind turbines, which is enough to supply around 4500 average EU households with electricity. [26] Obviously, this is very hard to implement on all already existing units, but it shows the potential energy saving even if it is made for a fraction of the units and for future units.

5.6 Cost

In addition to the performance results, it is important to take other aspects and side effects into account in the analysis. An important factor is the cost of operation. An AHU which is more efficient can provide the same required airflow rate but with less required motor power to drive the fans, resulting in saving expense on operation. However, as it was found in this study, an improved AHU is more advanced than the reference case, and thus requires both additional steps in the manufacture process as well as more material, most likely resulting in additional expense in the manufacturing and assembling process. Therefore it is necessary to make a detailed cost study to determine whether the saved expenses outweigh the added expenses.

6
Conclusion

The results obtained in this study are analyzed in order to connect to the tasks in the problem statement. The main issues with the current design are identified and located to three key regions of the AHU: the interaction, recirculation and the outer walls regions. Three modifications are created in order to improve the flow in these regions.

It is clear based on all observed parameters that efficiency improvements on the current AHU design are possible with implementation of all modifications presented in this thesis. The modifications offer improvement in all of the three regions of interest. In addition to this, they all show improvements in terms of static pressure and fan efficiency, with a potential increase between 1.54 and 2.08 % compared to the current design.

Comparison between the experimental testing and numerical simulations shows that the results are fairly similar for the fan efficiency, where the simulations are over-predicting the improvement compared to the experiments. However, the difference is considered small enough for the results to be considered valid. On the other hand, the static pressure differs significantly between the two methods, and could not therefore be validated for this parameter.

To answer the question which of the modifications is the best choice, is not straightforward. The static pressure results show that each operating point has a different best choice, while the fan efficiency results show that the modifications performs similar at all operating points, with small exceptions for operating points 1 and 3. Based on the contour plots of velocity and turbulent kinetic energy however, it is found that the curved wall generally outperforms the other two when analyzing the three regions of interest, due to its ability to handle the flow at the corners well. Therefore the main conclusion is drawn that the curved wall is the best option out of the modifications.

Bibliography

[1] EnviroVent Ltd. Five top reasons why your home needs good ventilation. https://www.envirovent.com/blog/five-top-reasons-why-your-home-needs-good-ventilation/. Accessed at 2020-12-02.

[2] Swegon. Radon in homes. https://www.swegon.com/guides/residential-ventilation/radon-in-homes/. Accessed at 2020-12-02.

[3] Official Journal of the European Union. *Commission Regulation (EU) No 327/2011 of 30 March 2011 implementing Directive 2009/125/EC of the European Parliament and of the Council with regard to ecodesign requirements for fans driven by motors with an electric input power between 125 W and 500 kW.*

[4] Official Journal of the European Union. *Commission Regulation (EU) No 1253/2014 of 7 July 2014 implementing Directive 2009/125/EC of the European Parliament and of the Council with regard to ecodesign requirements for ventilation units.*

[5] Official Journal of the European Union. *Directive 2009/125/EC of the European Parliament and of the Council of 21 October 2009 establishing a framework for the setting of ecodesign requirements for energy-related products.*

[6] Official Journal of the European Union. *Directive (EU) 2018/2002 of the European Parliament and of the Council of 11 December 2018 amending Directive 2012/27/EU on energy efficiency.*

[7] European Parliament. Energy: new ambitious targets on renewables and energy efficiency. https://www.europarl.europa.eu/news/en/press-room/20181106IPR18315/energy-new-ambitious-targets-on-renewables-and-energy-efficiency. Accessed at 2021-01-12.

[8] S. Serban Stankic and R. C. Ploesteanu. Investigation of the effect of multiple centrifugal fans close to each other in operation. Master's thesis, Chalmers University of Technology, 2019.

[9] F. M. White. *Fluid Mechanics.* McGraw-Hill, New York, 7th ed. edition, 2011.

[10] Siemens. STAR CCM+ User Manual. Wall treatment. Accessible with a STAR-CCM+ license.

[11] CFDsupport. Turbulent boundary layer. https://www.cfdsupport.com/OpenFOAM-Training-by-CFD-Support/node342.html. Accessed at 2020-09-24.

[12] Siemens. STAR CCM+ User Manual. Turbulence: K-epsilon model. Accessible with a STAR-CCM+ license.

[13] Wolfgang Rodi. Experience with two-layer models combining the k-epsilon model with a one-equation model near the wall. In *29th Aerospace sciences meeting*, page 216, 1991.

[14] T. H. Shih, W. W. Liou, A. Shabbir, Z. Yang, and J. Zhu. A new k-epsilon eddy viscosity model for high reynolds number turbulent flows: Model development and validation. 1994.

[15] L. Davidson. *Fluid mechanics, turbulent flow and turbulence modeling*. Department of Mechanics and Maritime Sciences, Chalmers University of Technology, Gothenburg, 2020.

[16] U.S. Department of Energy and AMCA. *Improving Fan System Performance: A Sourcebook for Industry.* Washington DC, 2003.

[17] R. W. Whitesides. *Basic Pump Parameters and the Affinity Laws*. PDH Center, Fairfax, VA, 2012.

[18] Air Movement and Control Association. Introducing fan efficiency ratios. https://www.amca.org/assets/resources/public/resources/FEG_Whitepaper_single%20pages.pdf. Accessed at 2020-12-02.

[19] Twin City Fan Companies Ltd. *Understanding Fan Curves - Fe-2000*. Minneapolis, 2018.

[20] ASHRAE. *2016 ASHRAE Handbook - Heating, Ventilating, and Air-Conditioning Systems and Equipment (SI Edition)*. American Society of Heating, Refrigerating and Air-Conditioning Engineers (ASHRAE), Inc., 2016.

[21] Pointwise. Compute grid spacing for a given y+. https://www.pointwise.com/yplus/. Accessed at 2020-09-23.

[22] Siemens. STAR CCM+ User Manual. Prism layer mesher. Accessible with a STAR-CCM+ license.

[23] LEAP Australia. Tips & tricks: Convergence and mesh independence study. https://www.computationalfluiddynamics.com.au/convergence-and-mesh-independent-study/. Accessed at 2020-10-19.

[24] Siemens. STAR CCM+ User Manual. 6-dof rigid body motion. Accessible with a STAR-CCM+ license.

[25] Swegon. Gold. https://www.swegon.com/products/air-handling/gold/. Accessed at 2021-01-14.

[26] The European Wind and Energy Association. Wind energy's frequently asked questions (faq). https://www.ewea.org/wind-energy-basics/faq/. Accessed at 2021-01-14.

A

Simulation models

Table A.1: Models used in the CFD simulations

Constant Density
Gas
Gradients
Gravity
K-Epsilon Turbulence
Realizable K-Epsilon Two-Layer
Reynolds-Averaged Navier-Stokes
Segregated Flow
Solution Interpolation
Steady
Three Dimensional
Turbulent
Two-Layer All y+ Wall Treatment
Wall Distance

B

Mesh settings

B.1 Inlet mesh

Table B.1: Inlet mesh - default control

Control	A	B	C	D
Target Surface Size	25.0	20.0	20.0	20.0
Minimum Surface Size	12.5	10.0	10.0	10.0
Surface Growth Rate	1.3			
Volume Growth Rate	1.2			
Prism Layer Near Wall Thickness	0.2			
Prism Layer Total Thickness	30.0			
Number of Prism Layers	15			

Table B.2: Inlet mesh - inner cone control

Control	A	B	C	D
Target Surface Size	5.0	4.0	4.0	4.0
Minimum Surface Size	5.0	4.0	4.0	4.0
Prism Layer Near Wall Thickness	0.02			
Prism Layer Total Thickness	10.0			
Number of Prism Layers	18			

Table B.3: Inlet mesh - inlet interface control

Control	A	B	C	D
Target Surface Size	5.0	4.0	4.0	4.0
Minimum Surface Size	5.0	4.0	4.0	4.0

B.2 Fan mesh

Table B.4: Fan mesh - default control

Control	A	B	C	D
Target Surface Size	5.0	4.0	4.0	3.0
Minimum Surface Size	5.0	4.0	4.0	3.0
Surface Growth Rate	1.1			
Volume Growth Rate	1.0			

Table B.5: Fan mesh - blades, inner backplate and inner shroud control

Control	A	B	C	D
Target Surface Size	5.0	3.0	2.0	1.5
Minimum Surface Size	5.0	3.0	2.0	1.5
Prism Layer Near Wall Thickness	0.05			
Prism Layer Total Thickness	2.0			
Number of Prism Layers	15			

Table B.6: Fan mesh - gap wall control

Control	A	B	C	D
Target Surface Size	5.0	4.0	4.0	3.0
Minimum Surface Size	5.0	4.0	4.0	3.0
Prism Layer Near Wall Thickness	0.04			
Prism Layer Total Thickness	0.43			
Number of Prism Layers	10			

Table B.7: Fan mesh - inlet interface control

Control	A	B	C	D
Target Surface Size	5.0	4.0	4.0	3.0
Minimum Surface Size	5.0	4.0	4.0	3.0

Table B.8: Fan mesh - outlet interface control

Control	A	B	C	D
Target Surface Size	5.0	3.5	3.0	2.25
Minimum Surface Size	5.0	3.5	3.0	2.25

Table B.9: Fan mesh - gap interface control

Control	A	B	C	D
Target Surface Size	1.25	1.0	1.0	0.75
Minimum Surface Size	1.25	1.0	1.0	0.75

B.3 Outlet mesh

Table B.10: Outlet mesh - default control

Control	A	B	C	D
Target Surface Size	12.5	8.5	7.5	7.25
Minimum Surface Size	12.5	8.5	7.5	7.25
Surface Growth Rate	1.3			
Volume Growth Rate	1.2			
Prism Layer Near Wall Thickness	0.1			
Prism Layer Total Thickness	20.0			
Number of Prism Layers	15			

Table B.11: Outlet mesh - vertical wall control

Control	A	B	C	D
Target Surface Size	5.0	3.5	3.0	2.9
Minimum Surface Size	5.0	3.5	3.0	2.9
Prism Layer Near Wall Thickness	0.2			
Prism Layer Total Thickness	10.0			
Number of Prism Layers	15			

Table B.12: Outlet mesh - outlet interface control

Control	A	B	C	D
Target Surface Size	5.0	3.5	3.0	2.9
Minimum Surface Size	5.0	3.5	3.0	2.9

Table B.13: Outlet mesh - outer shroud control

Control	A	B	C	D
Target Surface Size	1.25	0.85	0.75	0.725
Minimum Surface Size	1.25	0.85	0.75	0.725
Prism Layer Near Wall Thickness	0.05			
Prism Layer Total Thickness	3.0			
Number of Prism Layers	12			

Table B.14: Outlet mesh - outer shroud thickness control

Control	A	B	C	D
Target Surface Size	5.0	3.5	3.0	2.9
Minimum Surface Size	5.0	3.5	3.0	2.9
Prism Layer Near Wall Thickness	0.01			
Prism Layer Total Thickness	1.22			
Number of Prism Layers	12			

Table B.15: Outlet mesh - outer backplate control

Control	A	B	C	D
Target Surface Size	2.5	2.0	1.5	1.45
Minimum Surface Size	2.5	2.0	1.5	1.45
Prism Layer Near Wall Thickness	0.04			
Prism Layer Total Thickness	2.0			
Number of Prism Layers	12			

Table B.16: Outlet mesh - outer cone control

Control	A	B	C	D
Target Surface Size	5.0	3.5	3.0	2.9
Minimum Surface Size	5.0	3.5	3.0	2.9
Prism Layer Near Wall Thickness	0.05			
Prism Layer Total Thickness	5.0			
Number of Prism Layers	12			

Table B.17: Outlet mesh - wake refinement control

Control	A	B	C	D
Wake Refinement	12.5	8.5	7.5	7.25